AD NUMBER

AD911373

NEW LIMITATION CHANGE

TO

Approved for public release, distribution unlimited

FROM

Distribution authorized to U.S. Gov't. agencies only; Test and Evaluation; JUN 1973. Other requests shall be referred to Air Force Avionics Laboratory, Attn: NVN, Wright-Patterson AFB, OH 45433.

AUTHORITY

AFAL ltr, 12 Jan 1976

AFAL-TR-73-190

RF CLEANING-RING LASER GYRO

Gary D. Babcock and Fredrick Vescial
Autonetics Division of Rockwell International Corporation

TECHNICAL REPORT AFAL-TR-73-190

June 1973

AIR FORCE AVIONICS LABORATORY
Research and Technology Division
Air Force Systems Command
Wright-Patterson Air Force Base, Ohio 45433

NOTICE

When Government drawings, specifications, or other data are used for any purpose other than in connection with a definitely related Government procurement operation, the United States Government thereby incurs no responsibility nor any obligation whatsoever; and the fact that the government may have formulated, furnished, or in any way supplied the said drawings, specifications, or other data, is not to be regarded by implication or otherwise as in any manner licensing the holder or any other person or corporation, or conveying any rights or permission to manufacture, use, or sell any patented invention that may in any way be related thereto.

Copies of this report should not be returned unless return is required by security considerations, contractual obligations, or notice on a specific document.

RF CLEANING-RING LASER GYRO

Gary D. Babcock and Fredrick Vescial

FOREWORD

This document constitutes the final engineering report for the RF Cleaning-Ring Laser Gyro program. The effort was performed from 17 April 1972 through 28 February 1973, by the Autonetics Division of Rockwell International Corporation, 3370 Miraloma Avenue, Anaheim, California 92803. The data contained in this report were generated under Air Force Contract F33615-72-C-1741, Project No. 6095, for the Air Force Avionics Laboratory, under the monitorship of Robert W. McAdory (AFAL/NVN), Wright-Patterson Air Force Base, Ohio 45433.

This Technical Report has been reviewed and is approved for publication.

WILLIAM J. DELANEY, Colonel, USAF
Chief, Navigation and
Weapon Delivery Division

ABSTRACT

This document presents the results of RF Cleaning - Ring Laser Gyro program performed by the Autonetics Division of Rockwell International Corporation. One of the most significant problems confronting ring laser development is short life. The key to long ring laser life is a clean cavity (free of contaminants). The objectives of the contract were to test the RF cleaning concept and to build deliverable RLG hardware including both sensors and electronics.

The RF cleaning study was performed to determine the feasibility of using RF energy to clean ring laser gyro cavities. A "dual discharge" approach was selected as the most suitable RF coupling technique for cavity cleaning. Experimental studies were conducted to select and optimize cleaning parameters and procedures. Comparative effectiveness of cleaning techniques was measured by optical spectroscopy and by life test of operational ring laser instruments.

Data are presented which indicate that oxygen is the most efficient cleaning gas and that RF cleaning used in conjunction with normal thermal degassing processes can provide for improved laser gyro cleanliness. Conclusions and recommendations for future studies are also presented.

Instrument and electronic design of the deliverable hardware are described. Autonetics state-of-the-art design and processing techniques are incorporated in the sensor design. Operating procedures and test results obtained with the equipment at Autonetics are given. A summary is presented of brief studies conducted on RLG reliability, maintainability, and system safety.

CONTENTS

CONTENTS (Cont)

ILLUSTRATIONS

ILLUSTRATIONS (Cont)

TABLES

SECTION I

INTRODUCTION

The ring laser gyro has shown much promise as a high accuracy, low-cost, strapdown angular rate sensor for a wide variety of guidance applications. Its unique sensing mechanism and inherently simple structure should allow operation under high-g missile environments as well as under normal aircraft cruise conditions. The laser gyro theoretical limits on drift rate and maximum rotation rate appear to be considerably better than required for the present needs of navigation and guidance systems. Although ring lasers are still in the development stage, accuracies now being attained are sufficient for some applications. However, before the laser gyro can be used operationally, its lifetime must be significantly improved.

A program was devised to investigate a means to overcome one of the major factors known to limit laser gyro lifetime, namely residual contaminants on the interior surfaces of the laser cavity. Information from other sources suggested that improved cleaning to remove such contaminants could be obtained with an RF discharge in a selected gaseous medium. The work reported herein included first the development and evaluation of the RF cleaning technique, and then the fabrication of a operational laser gyro utilizing the cleaning process indicated to be optimum.

The lifetimes of ring laser gyro instruments are generally recognized to be limited by four factors: (1) gas contamination, (2) gas cleanup, (3) helium permeation, and (4) reflector degradation. Gas contamination may arise from residues left by inadequate cleaning during fabrication, outgassing from the materials of construction, decomposition of structural materials due to localized sputtering or plasma bombardment, and inward permeation of contaminants from external sources.

Gas cleanup is the loss of gas from the helium-neon lasing mixture due to diffusion or ion burial into internal surfaces and gettering effects of cathode sputtering. Helium permeation is the loss of this particular gas due to its relatively rapid diffusion through certain materials typically used for ring laser gyro construction, such as fused silica. Mirror degradation is caused by bombardment of the reflective surface by high energy particles from the plasma discharge in laser gyros.

Of these four categories, gas contamination appears to be the one which has the greatest practical effect in limiting laser gyro lifetime and which also is the least controllable by choice of materials or other design considerations. Furthermore, of the several causes of gas contamination, it is apparent that residues left from inadequate cleaning could have the most immediate and drastic influence with respect to degradation of laser gyro performance and termination of useful instrument life. For these reasons, the prospect of more effective cleaning by utilization of an RF energy discharge coupled into the laser gyro body interior was felt to be worthy of investigation. A significant improvement in cleaning with the RF technique would contribute directly to the operational lifetime capability of ring laser gyros.

The approach which was pursued with the RF cleaning studies was first to investigate the techniques for application of the method to ring laser gyros, then to optimize the process, and finally to evaluate its effectiveness by means of analytical techniques and life tests. An important consideration throughout was how RF cleaning

would relate to the existing cleaning procedures generally established for ring laser gyro fabrication. The objective was to have RF cleaning complement the conventional processing procedure so as to obtain the most beneficial net effect.

The second part of this program was to fabricate a ring laser gyro complete with operational and test electronics suitably packaged for laboratory tests at Holloman Air Force Base. The objective of this effort was to supply for evaluation prototype hardware to represent the state-of-the-art ring laser gyro technology available at Autonetics. Accordingly, the hardware was designed and fabricated based on concepts existing at the time for laboratory testing applications only, and involved no development effort relative to packaging for adverse or variable environments.

The RF cleaning studies had progressed to the point that it was possible to utilize essentially the final method developed on this program for cleaning of the ring laser gyro instrument during its fabrication. The results observed indicated that RF cleaning did contribute to a more effective and stable laser gyro instrument.

SECTION II

RF CLEANING STUDIES

1. INTRODUCTION

With the present state-of-the-art techniques, gas contamination appears to be the primary limiting factor for long shelf life and the cause for short-term operating failures in ring laser gyros. The laser cavity gas may become contaminated by inadequate cleaning techniques during construction, outgassing from the materials and bonds used in the gyro, and, under certain conditions, by inward diffusion of external contaminants.

The common technique for reduction of gas contamination sources is to thermally degas the entire instrument through high temperature vacuum baking. Adhesive seals and optical coatings generally limit the baking temperature in ring laser instruments so that impurity outgassing becomes a very time consuming and costly process.

The primary objective of this study was to investigate cleaning ring laser gyros by a new process that has the potential of producing cleaner cavities in much less time and at a lower cost. The technique involves coupling RF energy into a gas-filled laser cavity so that a discharge will be sustained where ions bombard the wall and entire inner surfaces of the instrument. Such an RF energy cleaning process was first developed and successfully used to clean helium magnetometers. Since both instruments employ gas-filled cavities constructed of similar materials,the process should be applicable to the ring laser gyro.

The experimental approach to the investigation was to (1) evaluate techniques for efficiently coupling RF energy into the ring laser cavity, (2) select and optimize cleaning parameters, gases, and an RF coupling network, and (3) determine the effectiveness of the RF cleaning technique through the processing and comparative lifetime testing of several operational ring laser instruments. Considerable emphasis was also placed on optical spectroscopy as a technique for monitoring laser cavity cleanliness and for identifying types and amounts of contaminants. A detailed description of the technical tasks and specific experiments performed during the study are presented in the following sections. The final section discusses the results of the investigation and lists specific conclusions and recommendations for further work.

2. RF COUPLING TECHNIQUES

A series of tests were performed on several ring laser instruments and straight laser tubes to determine the best RF coupling technique for the cleaning studies. The following approaches were evaluated: (1) inductive coupling with a coil completely surrounding the instrument, (2) capacitive coupling through two parallel plates sandwiching the instrument, and (3) direct RF contact coupling through anodes, cathodes, getter pins, and other feedthrough areas. Three different RF power supplies available from laboratory test equipment were used for these tests. Frequencies of 13.67 MHz and 40.68 MHz could be generated with this equipment.

Each of the RF coupling techniques evaluated were able to sustain an RF discharge in the reservoir area of the tubes under several different power conditions and efficiencies. However, difficulty was encountered in sustaining an RF discharge in the bore areas of the ring laser. In a conventional straight laser tube, the bore usually consists of a relatively thin wall capillary tube which is separated from the cathode-reservoir section. This capillary can be surrounded with a network of RF electrodes and an RF discharge can be readily coupled into the bore region. In a ring laser gyro employing single-block construction, the bores are drilled into the block itself and buried in a thick wall of body material. Apparently, the field drop through these walls is sufficient to limit RF discharge conditions in the bore.

An RF discharge could not be sustained in any of the bore areas of a ring laser instrument when inductively coupled with a coil. However, the corner portions of the instrument and nearby bore sections could be discharged via capacitive plate coupling. These corner areas are somewhat enlarged to accommodate reflector mounting and provide a thinner wall area for better field coupling. The bore areas could be discharged by direct RF contact from anode to anode or to an external accessory electrode. Considerable heating of the anodes was found to occur, however, and in one case the adhesive used to mount the anode failed, generating a small leak in the gyro. Direct RF coupling through feedthrough pins has also been noted to melt or fracture metal-to-glass seals.

It was determined that for the present ring laser cleaning experiment, the optimum field coupling and wall bombardment conditions will be best achieved with simultaneous DC and RF discharge. Here, the technique employed is to utilize the normal DC discharge which operates the instrument in conjunction with an externally coupled RF field. The RF field can be applied via a coil inductively coupling the instrument or by capacitive plate coupling. Under normal DC operating conditions, the plasma is confined to a portion of the interior of the instrument cathode and to the central region of the tube bores. With additional RF excitation, the discharge spreads to the wall areas of the bore and completely fills the gain section of the tube. In addition, the entire reservoir area undergoes excitation due to the RF field. Thus, all the interior surfaces of the ring laser instrument undergo bombardment without excessive localized heating. The capacitive coupling technique appears to be the optimum one for applying the RF field under this dual discharge condition. Inductive coupling is satisfactory for small-size tubes, but the larger ring laser instruments (40 cm) require very large coils in which it becomes very difficult to achieve resonance conditions.

Capacitance coupling to the ring cavities was best accomplished by sandwiching the instrument on top and bottom with two electrode plates. The plate configuration used for 15-cm path length ring laser gyros is shown in Figure 1. Holes were cut in the top plate to accommodate the getter and cathode pin feedthroughs. Similar plates were utilized for larger size instruments.

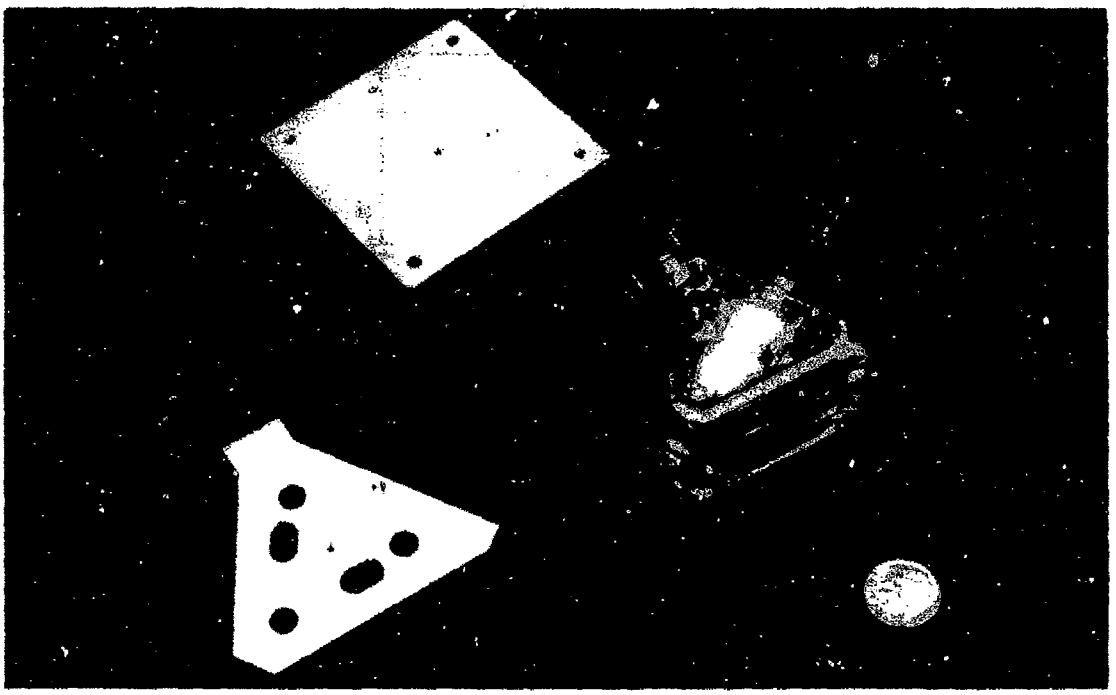

Figure 1. 15-cm Ring Laser Gyro and Plates Used for Capacitive RF Coupling

3. RF NETWORK SELECTION

In order to capacitively discharge the gas-filled section of the ring laser during the filling procedure, a high-voltage excitation is required. The voltage level required is not available from standard RF supplies, since these are designed to drive a nominal 50-ohm load. Therefore, a conversion circuit was designed and fabricated which converts the low-voltage high-current output into a high-voltage low-current source. The circuit is basically a balanced inductively coupled parallel-tuned tank that is driven by a series-tuned circuit. The output of the tuned tank circuit has voltages exceeding 400 volts. This level is sufficient to cause the gases in the plasma to spontaneously discharge. The balanced circuit operates at half the voltage to ground of the normal π circuit. Since RF radiation losses are proportional to the voltage squared, the circuit has about one-quarter the radiation loss. Figure 2 shows the schematic of the balanced circuit. L_1 and L_2 constitute a transformer which is necessary to obtain double-ended output. C_2 is a butterfly capacitor that maintains ground halfway between the two output electrodes. C_2 is taken as the combined capacitance of the plate electrodes and butterfly capacitor. R' is the effective load the circuit must match. In operation, L_2 and C_2 are approximately in resonance, $\omega_2 L_2 C_2 \approx 1$. The circuit is used in conjunction with a Spectra-Physics Model 200 RF power supply. The supply runs at 40.68 MHz and has a maximum power output level of 40 watts. Two parallel aluminum plates were used to sandwich the gyro body on top and bottom for capacitive coupling.

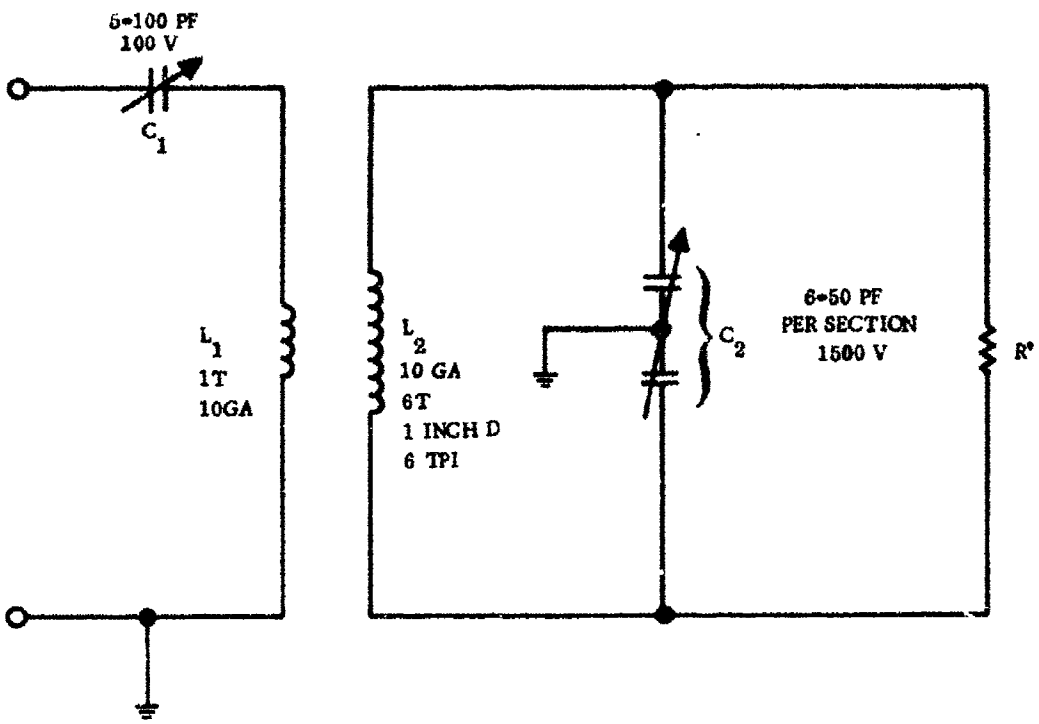

Figure 2. Schematic of Balanced RF Tuning Circuit

The optimum RF network circuit components were selected by trial and error tuning with the aid of a Johnson Direction Coupler. The directional coupler consists of two indicating circuits placed back to back that are coupled to the center conductor of a short section of transmission line. The combination of inductive and capacitive coupling is such that the incident power is cancelled out and the indicator circuits measure relative reflected power. Since the indicators are back to back, one measures actual reflected power and the other measures actual incident power, which because of the indicator circuit placement appears to be reflected to the coupler. The ratio of reflected power to incident power is used to determine the standing wave ratio (SWR) which can be directly metered with the Directional Coupler. For maximum power absorption by the load, minimum power losses in the cable and efficient operation of the exciter, the standing wave ratio should be as close to one as possible.

Figure 3 displays the exciter, directional coupler, standing wave ratio meter, tuning circuit and capacitive coupling apparatus that were used for the RF cleaning studies. The component values that were utilized for coupling RF energy on to the 15-cm size ring laser gyros are shown in Figure 2. Coupling into larger size instruments could be achieved with the same basic circuit by merely increasing the number of turns on L_2.

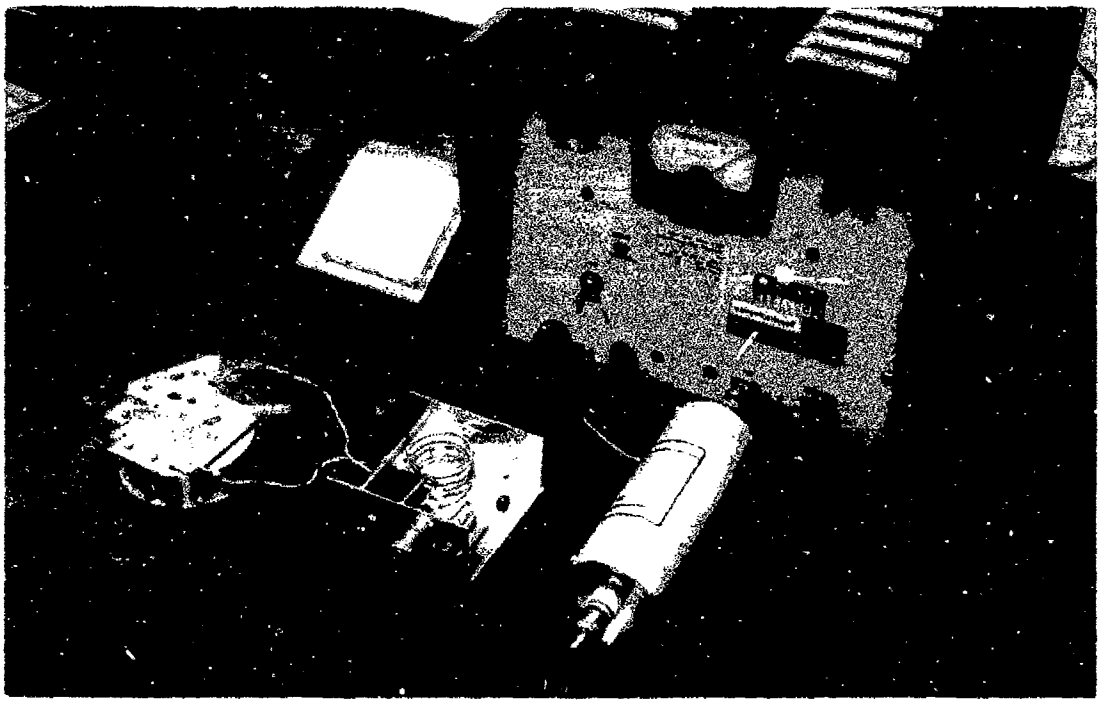

Figure 3. Exciter, Directional Coupler, Standing Wave Ratio Meter, Tuning Circuit and Capacitive Coupling Apparatus for RF Cleaning Studies

4. MEASURING CLEANING EFFECTIVENESS

In order to optimize the parameters and procedures of the RF cleaning experiment, it was necessary to establish the levels to which cleanliness could be monitored in a ring laser gyro instrument. Both optical and mass spectroscopy were considered as possible techniques for measuring cleaning effectiveness. The optical spectrograph approach was selected as the most suitable one for the present RF studies since continuous impurity analysis could be conducted under operational conditions both on and off the fill stand without removal of fill or cleaning gases for sampling purposes.

The radiation emitted by matter in the plasma state may exhibit either a continuum or line spectra or both. Its analysis by spectroscopic measurements of continuum intensities, line intensities, and line profiles can often provide considerable information about plasmas. The frequencies of the lines emitted from an excited atom or molecule are characteristic of the atoms or molecules themselves, while the shape of the line indicates the environmental effects on the emitter.

The emission of a spectral line is determined by the population of the upper quantum level of the line and by Einstein's transition probabilities. Thus, from the intensities of the individual lines, the density of atoms in upper states of the lines can be calculated if the transition probabilities are known. A continuous emission spectrum is always formed when at least one of the respective quantum states is a free state, the energy of which is in a continuum of permitted values. Continuum radiation can thus

be due to free-free or bound-free transitions, and the emitted intensity is proportional to the product of the electron density and the ion density. Continual continua may also be formed by merging of unresolved lines or lines which are close to each other and very broad. Such continua are called apparent continua.

The optical spectrum of a helium-neon plasma is complex due to the strong emission characteristics of neon. The spectrum consists of numerous discrete and intense lines which often make it difficult to monitor minor transitions from impurity elements. Figure 4 displays the spectrum of a partially contaminated helium-neon filled ring laser gyro. The numbers associated with each of the peaks are from dial readings taken from the spectrophotometer and may not precisely correspond to exact spectral wavelengths. All the peaks in Figure 4 can be identified with either neon or helium except for the 6563 Å line (circled) which is associated with hydrogen. The intensity of this hydrogen transition corresponds to approximately 0.3 percent contamination of the helium-neon gas in the ring laser gyro.

A series of experiments was conducted to determine minimum detectable spectral transition levels for several likely ring laser gyro contaminants. The experimental technique was to: (1) determine all spectral transitions associated with helium and neon, (2) identify major spectral peaks for each of the likely contaminant materials, and then (3) examine the optical spectra of normal helium-neon fill gases with known amounts of impurities added. The impurity gases monitored were hydrogen, oxygen, nitrogen, air, water vapor, and argon. Acetone and methyl alcohol were also evaluated as representative of organic type impurities. All of these materials are likely to be found in various types of contaminated instruments. Laser power output was also measured during the detection level tests to provide a measure of gain degradation under varying impurity conditions.

A 40-cm ring laser gyro was used for the impurity detection experiments. This instrument was a previously assembled unit which was refurbished with a new cathode-reservoir assembly. Initial attempts to monitor optical spectra were made with a hand-held spectrometer consisting of a set of simulated diffraction gratings. This technique was useful for quick visual monitoring of large amounts of contaminant gases. However, it was found to be extremely difficult to visually pick out small impurity transitions because of the strong emission characteristics of neon. Also, many of the likely contaminants possess transitions that are beyond the visible spectrum. A high-resolution scanning monochrometer is the most suitable type of instrument for impurity detection measurements.

The Jarrell-Ash scanning spectrophotometer pictured in Figure 5 was used to monitor optical spectra for the impurity tests. This unit automatically scans the spectral region from 3500 Å to 8500 Å with better than one angstrom unit resolution. Both the ring laser gyro and spectrophotometer were attached to the gas fill station as shown in Figure 6.

The vacuum evacuation portion of the fill stand employs a trapped-oil diffusion pump capable of pumping below 1×10^{-8} torr. The fill station is equipped with a set of throttling valves for admission of precise amounts of external gases as well as helium and neon fill gases. Pressure levels are measured by a capacitance manometer with a range of 0.001 to 10 torr. Thus, impurity levels down to 100 ppm (by pressure) could be achieved by direct fill methods. Impurity levels to 1 ppm and lower could be achieved by successive dissolution techniques.

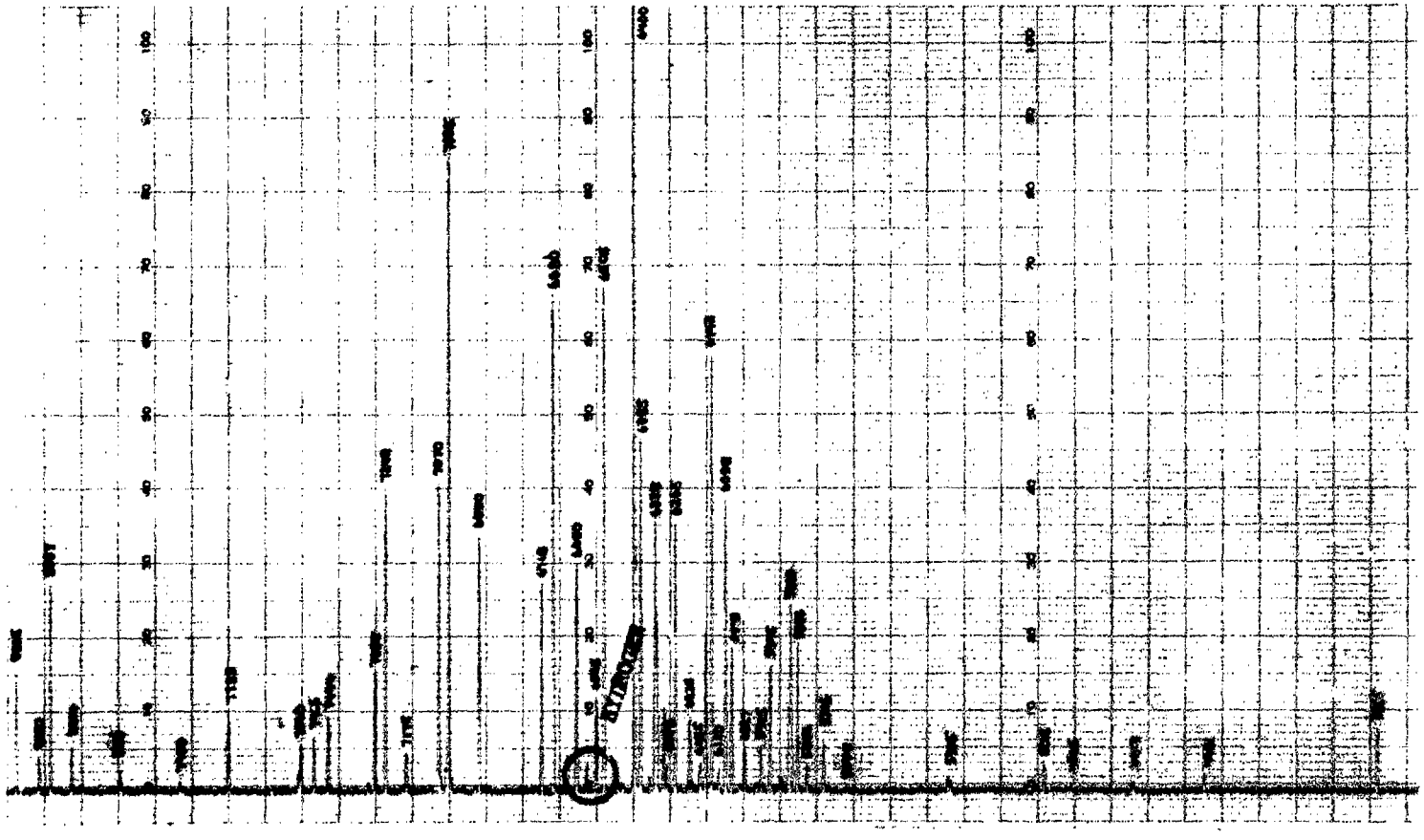

Figure 4. Optical Spectrum of a Partially Contaminated Helium-Neon Filled Ring Laser Gyro

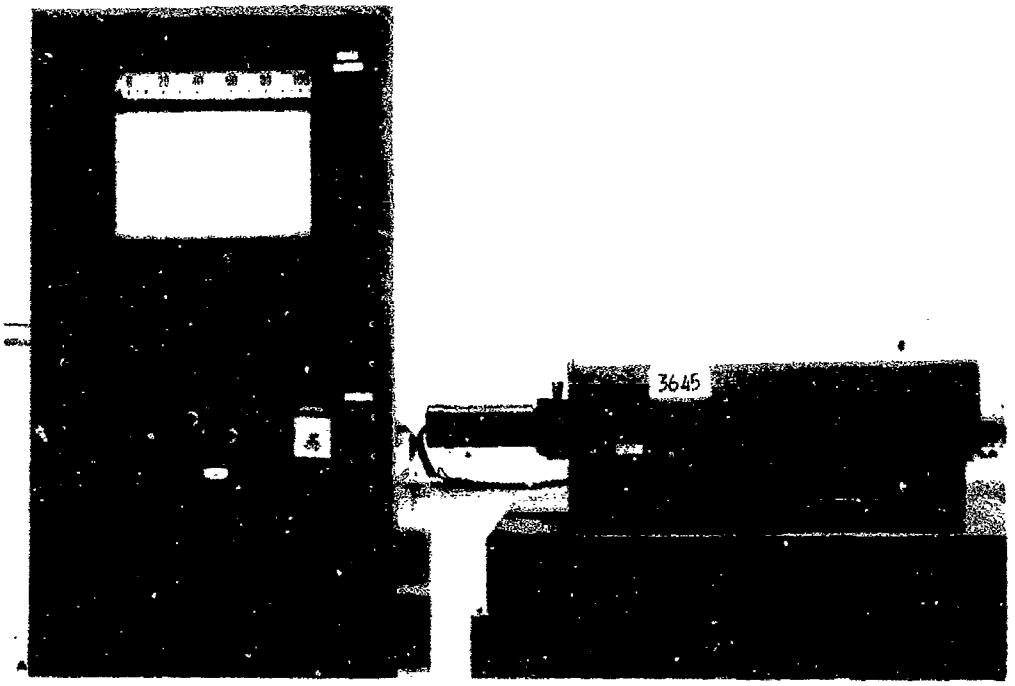

Figure 5. The Jarrell-Ash Scanning Spectrophotometer Used To Measure Optical Spectra of Impurities During RF Cleaning Experiments

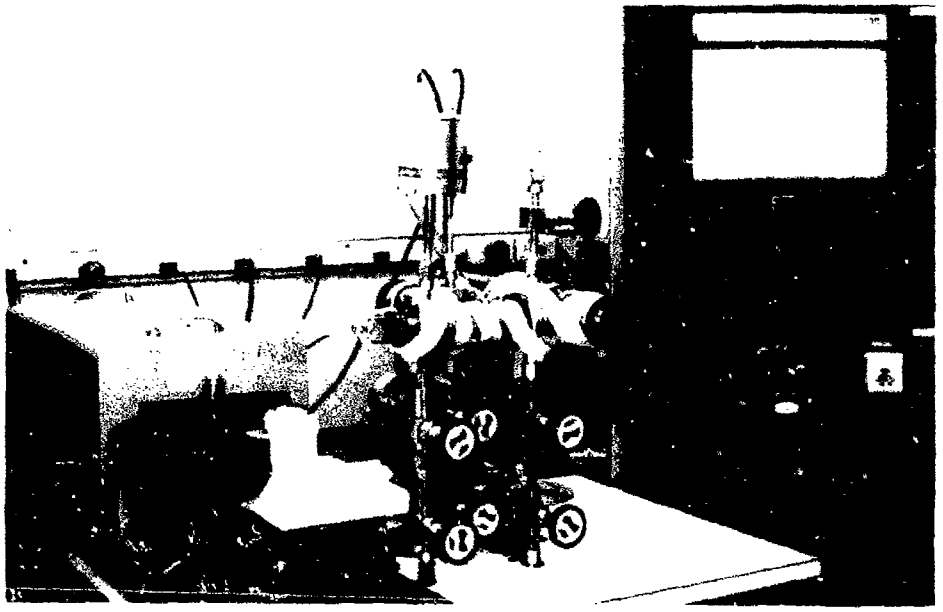

Figure 6. Ring Laser Gyro on the Gas Fill Stand Along With the Jarrell-Ash Scanning Optical Spectrometer

Optical spectra were initially generated for the helium-neon mixture (90 percent He^4, 10 percent natural Ne), for neon in a 1:1 isotopic ratio of Ne^{20}/Ne^{22}, and for He^3. The latter two are normally used as the final fill gases in an operational ring laser gyro instrument. The major spectral peaks of each of the fill gases were identified. Relative peak intensities were found to be very dependent upon fill pressures. Fill pressures of 2.5 and 6.0 torr were selected as a reference for all spectral data. The spectrum of He^3 was found to be very similar to that of He^4 with no additional peaks and with only minor changes in relative peak intensities. The spectrum of the mixture of neon isotopes was also very similar to that of natural neon.

Minimum detection levels and spectral characteristic of the impurity materials were as follows:

1. Hydrogen. The optical spectrum of hydrogen is identified by a major, well defined peak at 6563 Å. The transition is a very strong one and tends to dominate the spectrum even when additional impurity elements are present. The detection level of hydrogen, as a singular impurity, is approximately 30 ppm. However, several other likely ring laser gyro contaminants have hydrogen related transitions which limit the minimum detection level to a few hundred ppm under mixed impurity conditions.

2. Oxygen. The spectrum of oxygen was found to be considerably different from the normally published values taken under discharge conditions. The spectrum consisted of a general continuum over the scanned spectral interval with only two distinct, but minor peaks. A single peak was observed at 844 Å with a doublet occurring at 7771 Å and 7774 Å, respectively. When 10 percent oxygen was added to the normal helium-neon fill, the two discrete spectral peaks increased in amplitude by a factor of four. Successive dissolutions decreased peak intensities. The presence of large amounts of oxygen greatly attenuates the normally strong helium-neon spectra. However, the oxygen transitions are greatly attenuated with the addition of other impurities, particularly hydrogen. Oxygen alone can be detected in the helium-neon gas fill down to approximately 100 ppm.

3. Nitrogen. The spectrum of nitrogen is characterized by a large number of both minor and major spectral peaks. The major lines show broad leading edges due to associated minor spectral transitions and are readily identifiable. The line at 6723 Å is the most pronounced one for impurity detection measurements. Minimum detection levels were measured to be slightly below 200 ppm.

4. Air. The presence of air in the gyro gas fill is characterized, as one might expect, by major spectral peaks associated with nitrogen and oxygen and by minor peaks associated with argon. The detection sensitivity for air contamination is primarily defined by the spectral transitions related to nitrogen. To detect low impurity levels and to distinguish a pure nitrogen source from an air leak, the spectral transitions associated with argon also have to be monitored.

5. Argon. The detection sensitivity for argon as an impurity contaminant in the helium-neon plasma was measured to be approximately 25 ppm. This was the lowest measured value of all the potential contaminant materials that were tested. Argon is not expected to be a normal ring contaminant unless a leak occurs at one of the seals. Its high detection sensitivity, along with the fact that it is not usually getterable, makes it the prime candidate for monitoring gyro leaks.

6. Water Vapor. The presence of water vapor is evidenced by spectral peaks corresponding to hydrogen and oxygen. The hydrogen peak at 6563 Å and the oxygen doublet at 7774 Å generally occur in the amplitude ratio of 7/1 when water vapor is present as a contaminant. Variations of oxygen and hydrogen from this ratio usually indicate the presence of additional oxygen or hydrogen related impurities.

7. Organic Impurities. Organic contaminants in the ring laser gyro gas fill are identified by spectral peaks associated with hydrogen and oxygen. The ratio of hydrogen to oxygen is a function of the type of organic impurity. Acetone, for example, is characterized by an extremely large hydrogen peak with virtually no detectable oxygen. Methyl alcohol, on the other hand, shows a moderate hydrogen peak with a small but distinguishable oxygen transition. Apparently, organic materials are dissociated under plasma conditions. The amount and nature of the constituents liberated are related to the bond structures of the individual materials. The presence of an organic material in the plasma can be detected by measurable variations in the minor spectral peaks of both oxygen and hydrogen. However, the identification of the specific type of organic impurity is extremely difficult to establish with optical spectroscopic techniques alone.

Relative amplitudes of impurity transitions as a function of percentage gas contamination were also established during the impurity detection experiments. The results for argon, nitrogen, hydrogen, and oxygen are displayed in Figure 7. One can note that both argon and hydrogen possess fairly intense impurity transitions. Nitrogen and oxygen, on the other hand, provide small amplitude transitions which greatly limit the minimum detectable levels. Examination of the transition intensity curves for both the oxygen doublet (7771, 7774) and single transition (8446) indicate a crossover point at approximately 0.1 percent contamination with the doublet providing better detection sensitivity at the lower impurity levels. The percentage contamination curves in Figure 7 for oxygen were generated by direct fill techniques. Generating similar curves by dissolution techniques involving filling the instrument directly to a known contaminant level then reducing the level by pumping out a portion and adding additional He-Ne, did not prove successful due to a residual level of oxygen that remained in the tube. Apparently under oxygen discharge conditions a considerable amount of oxygen is absorbed and ion-implanted in the ring laser gyro cathode and/or body material. Such oxygen desorbs very slowly with time and requires a considerable period to pump out. This effect was also noted in the life-test portion of the program and is discussed further under that subject.

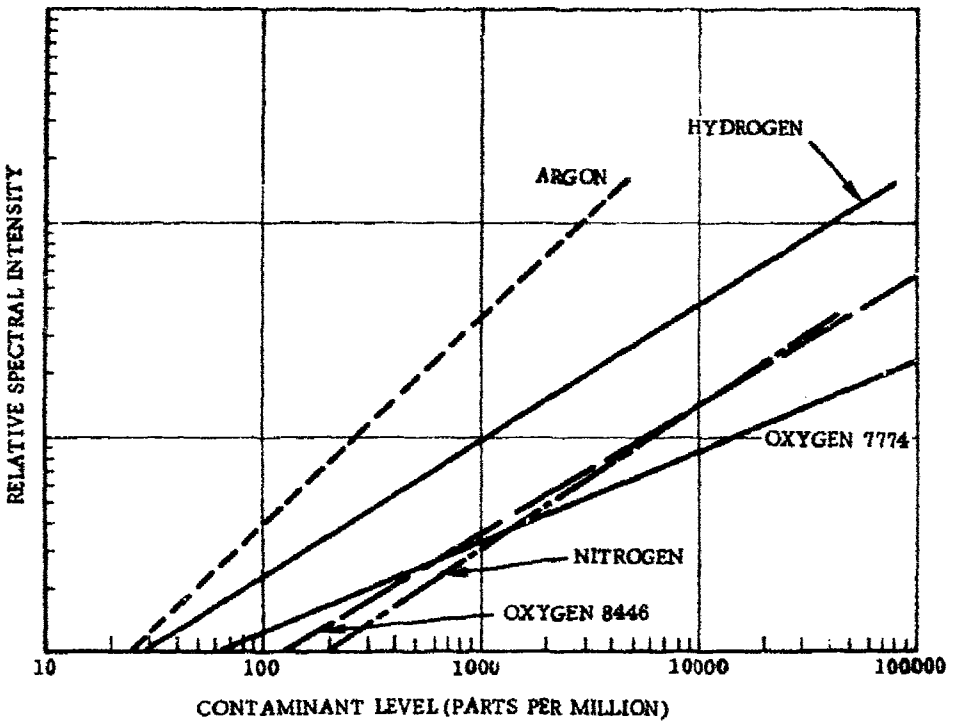

Figure 7. Relative Spectral Intensity as a Function of Concentration for Selected Impurity Gases

It was observed in all cases that contaminants attenuate the total spectrum of helium-neon. The attenuation of several strong neon transitions for varying amounts of hydrogen are displayed in Figure 8. The attenuation profiles of the neon 6532 Å line with respect to hydrogen, oxygen, and nitrogen are displayed in Figure 9. These curves indicate that hydrogen shows complete attenuation at lower levels than both nitrogen and oxygen. This is in agreement with the power output measurements of gain degradation which indicated that laser quenching was most sensitive to hydrogen impurities. Small amounts of oxygen had little effect on laser output and in some cases appeared to enhance laser gain. The attenuation profile of the 6328 Å line was found to be similar to the 6420 Å line. Continuous monitoring of the spontaneous emission from this transition which provides the stimulated laser output offers a means for direct measurement of laser gain as a function of contamination sources.

The experiments to establish minimum impurity detection levels with optical spectroscopy indicate, in general, that the presence of contaminants in the normal ring laser fill gas can be detected to a level of a few parts per million. The identification levels of specific impurities are in the range of 20 to 55 ppm depending on the type and/or combination of materials involved. These levels of detection provided a satisfactory base for monitoring the effectiveness of cleaning processes and procedures and also for optimizing the parameters of the RF cleaning experiments. In addition, the ability to identify different impurities under operational conditions enabled continuous impurity analysis during the life-test portion of the program.

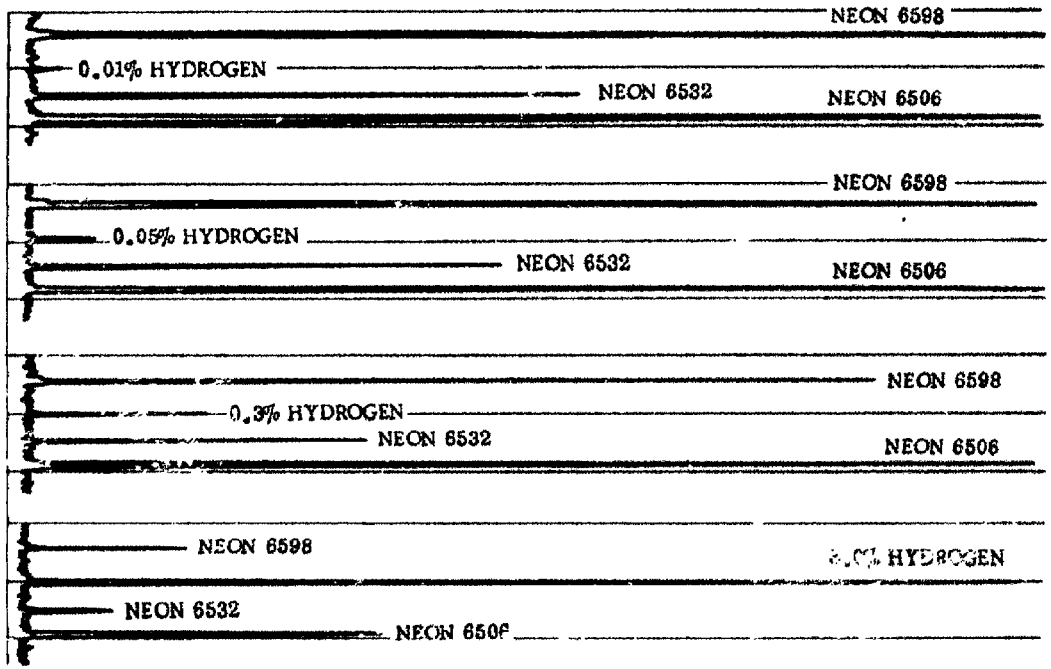

Figure 8. The Attenuation of Neon Spectral Lines by the Presence of Various Amounts of Hydrogen

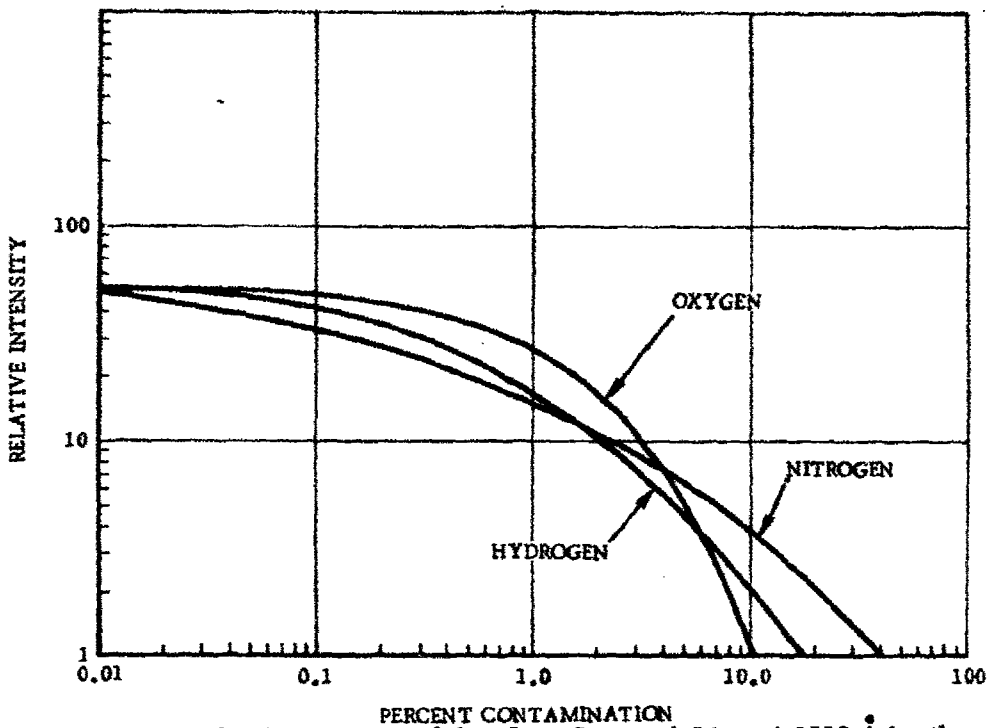

Figure 9. The Attenuation of the Neon Spectral Line at 6532 Å by the Presence of Hydrogen, Oxygen, and Nitrogen

5. CLEANING PARAMETERS

In glow discharge cleaning, removal of impurities is brought about by one or more of the following mechanisms:

1. Heating due to impingement and recombination of charged particles.
2. Impurity desorption due to electron bombardment.
3. Impurity desorption due to low energy ion bombardment.
4. Volatilization of organic residues by chemical reaction.

All of these factors were taken into consideration when selecting the optimum parameters for RF cleaning.

Both the bombardment and heating effects of the RF discharge were found to be greatly dependent on cleaning gas fill pressure. The optimum pressure was taken to be the point of most efficient coupling of the RF field into the laser cavity. This optimum pressure was slightly different for each type of cleaning gas.

A series of tests was conducted on a 15-cm ring laser gyro in which RF coupling was measured as a function of cleaning gas pressure. The efficiency of coupling was determined by measuring the tuned standing wave ratio of the RF network. Coupling effects could also be monitored visually by observing to what extent the RF discharge

completely filled the reservoir section of the ring laser gyro. Measurements were taken over a pressure range from 10 to 0.1 torr for several likely RF cleaning gases. Optimum pressures for RF couplings under dual DC and RF discharge conditions were as follows:

Helium (He^3)	-	8.5 torr
Argon	-	1.0 torr
Oxygen	-	6.0 torr
He^4-Ne^{20}	-	7.0 torr
Nitrogen	-	3.0 torr
Neon (Ne^{20}-Ne^{22})	-	6.0 torr

These differing optimum coupling pressures are no doubt related to atomic diameters, mean free paths, ionization potentials and ionization characteristics of the respective gases.

As one might expect, the amount of heating of the gyro surfaces due to particle bombardment is directly related to how efficiently the RF field is coupled into the cavity. A set of comparative time-temperature relationships was established to determine the heating effects of likely cleaning gases under optimum RF coupling conditions. The measurements were taken at the optimum RF coupling pressures previously listed at a constant power input level of 25 watts. A plot of temperature rise versus cleaning time is displayed in Figure 10. The temperatures indicated in the figure are those of the fused silica ring laser gyro body and were measured with a thermocouple taped to the exterior of the instrument near the bore area. One can note that thermal equilibrium occurs approximately 60-min after the initiation of the RF discharge for each of the gases. The reactive gases (oxygen and nitrogen) appear to generate larger heating effects than the inert gases.

The temperature of the fused silica reservoir cover of the ring laser gyro was also measured after the 60-min cleaning cycle. It was found to be 75°F hotter than the side wall temperatures indicated in the figure. This is no doubt due to the fact that the reservoir cover is normal to the applied RF field and receives maximum energy from bombardment effects. Also, radiation losses are considerably less than on the side walls due to the fact that the cover is somewhat shielded by the top capacitance coupling plate. The internal surface temperature of the gyro is probably much higher than either of the measured external temperatures and should provide for considerable thermal degassing. Ideally, the exterior of the gyro should be heated to its thermal limit (350°F) to also provide for maximum volume outgassing of the fused silica. This was readily accomplished by increasing the RF power into the cavity. Under maximum available power conditions (40 watts) utilizing oxygen cleaning gas, the temperature of the instrument cover increased to over 400°F in 35-min. This is past the breakdown temperature of the epoxy cement used to seal the ring laser gyro body. In fact, during such a cleaning cycle a cement failure occurred at a getter pin feed through, resulting in a gyro leak. Approximately 32 watts of RF power were found to heat the gyro within safe baking limitations within a 60-min period. These conditions were selected as optimum for the subsequent gas selection experiments.

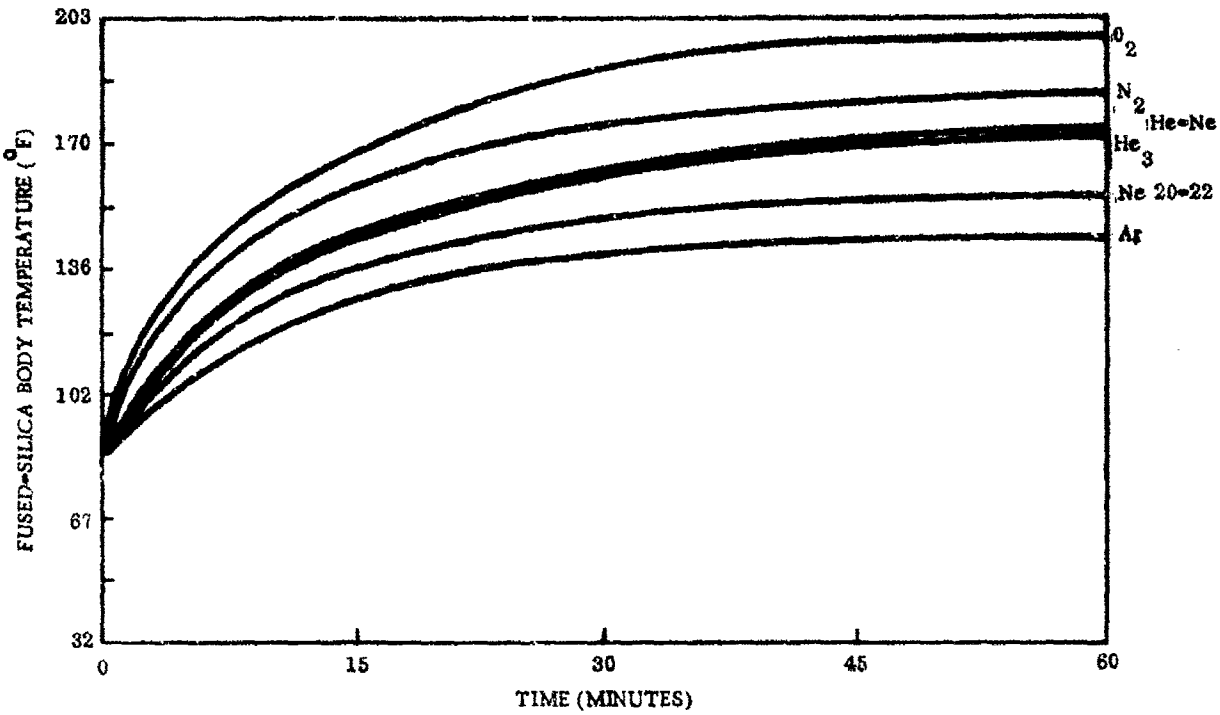

Figure 10. Temperature Rise Versus Time for Different RF Cleaning Gases

The experiments to select the optimum gas for the RF cleaning process consisted of monitoring impurity levels before, during, and after RF cleaning. In this way the effectiveness of each cleaning material could be directly determined. The gases evaluated were oxygen, nitrogen, helium, Ne^{20}-Ne^{22}, and argon. He^4 - Ne^{20} was used as the standard fill for measuring reference impurity spectra before and after filling with each of the cleaning gases. These initial tests were conducted with a single 15-cm ring laser gyro under the optimum pressure and coupling conditions described earlier. Laser power output was also monitored after each selection test. Equivalent starting conditions were achieved by venting the instrument to air for a specified period before cleaning.

Prior to any cleaning, the optical spectra from the 15-cm test instrument generally indicated approximately 1000 ppm of contaminant gases in the helium-neon fill mixture. The instrument did not lase under these conditions. During RF cleaning considerable amounts of observable contaminants were liberated. At the end of the cleaning period the contaminant level was found to be greater than 1 percent of the total fill. The primary impurity materials that were observed in each of the spectra were hydrogen and oxygen with an occasional trace of nitrogen.

Dual DC and RF discharge cleaning with helium gas appeared to liberate extremely large quantities of hydrogen with only moderate oxygen liberation. Argon cleaning showed a fairly large liberation of both hydrogen and oxygen. The neon isotopic mixture showed low impurity gas liberation effects with larger hydrogen evolution than oxygen. RF cleaning with oxygen showed virtually no hydrogen liberation. However, the spectrum of pure oxygen is a very diffuse one and may somewhat attenuate the

hydrogen transitions. Cleaning with nitrogen liberated considerable quantities of oxygen with smaller amounts of hydrogen.

Spectra taken either after pump-out and refill with the helium-neon mixture all showed trace amounts of either hydrogen and/or oxygen for all cleaning gases. Argon showed slightly lower trace contaminant amounts than both helium and neon. The reference spectra taken after oxygen cleaning, pump-out, and refill showed no detectable hydrogen but considerable amounts of remanent oxygen. Hydrogen attenuation due to oxygen was not observed in earlier helium-neon reference spectra were both impurity materials were in moderate amounts (<1000 ppm). Thus, the hydrogen removal may be a real effect. The large amount of remanent oxygen noted after RF oxygen cleaning was observed in the impurity detection experiments and can probably be explained by the reactive nature of the gas in that it tends to more readily enter into sorption-desorption types of interactions. The spectra taken after nitrogen cleaning showed very small hydrogen impurities but notable oxygen content. This is also probably due to the slow desorption characteristics of oxygen and is related to the considerable oxygen liberation observed during the RF nitrogen cleaning cycle.

The power output measurements taken after the different RF cleaning cycles were somewhat inconsistent with the impurity content observed in the optical spectra. In particular, lasing intensity was observed to be greatest after oxygen cleaning, even with moderate amounts of oxygen impurity still evident in the gyro. This can possibly be attributed to the removal of hydrogen by the oxygen cleaning process, since hydrogen has been found to be the impurity material to which laser gain reduction is most sensitive. Also, small amounts of oxygen impurity may actually enhance lasing intensity. The power output of the test ring laser gyro after RF cleaning with the other gases was down by a factor of 3 to 5 from the oxygen value.

6. COMPARATIVE LIFETIME TESTS

A second series of selection experiments were conducted in which the candidate cleaning gases were evaluated with several different ring laser gyro instrument assemblies, one for each candidate gas. These experiments provided for equivalent starting conditions and allowed for direct comparative evaluation of RF cleaning effectiveness under operational conditions. Four gases were evaluated: argon, helium, oxygen, and nitrogen. Argon is the gas that has been traditionally used for normal DC glow discharge processing. It is inert, relatively low cost, and, since it has a relatively heavy molecular weight, provides efficient high energy bombardment. Helium possesses several extremely high energy transitions in the lower end of the ultraviolet spectrum and thus may be very effective in dissociating and liberating surface absorbed impurities. Oxygen and nitrogen are reactive materials which may be useful for clean-up of hydrocarbon-type impurities.

The instruments used for the comparative life-tests were 15-cm pathlength ring laser gyros similar to the one shown in Figure 1. Selection of the 15-cm pathlength size for the life-test study was based primarily on the availability of gyro bodies and components. In addition, these instruments have comparatively small sized reservoirs and possess large surface area-to-volume ratios which should make gas contamination sources more distinguishable in shorter time intervals. The life-test ring laser gyros were previously assembled instruments that were stripped, recleaned, assembled, and rebuilt with new cathodes, mirrors and gettering assemblies for the life-test study. All the instruments were operated at the 1.15 μm infrared lasing transition. The gyros utilized aluminum cathodes and were equipped with two DC fired barium getters. Each unit employed a flat output mirror, a curved mirror, and a diaphragm-type mirror such that the cavity length could be tuned with a piezoelectric element.

Equivalent sets of mirrors were used on three of the units, designated RF-1, RF-2, and RF-4, so that each cavity supposedly had similar optical losses with corresponding laser output. The fourth unit, RF-4, employed slightly different curved and output mirrors which would result in somewhat lower laser output intensities.

A special epoxy resin was used to seal the components and covers to the ring laser gyro bodies.

Each of the life-test instruments was RF cleaned according to the following procedure.

1. Attach the ring laser gyro to the gas fill station and evacuate for a 3-hr period.
2. Flush the ring laser gyro with cleaning gas and pump out.
3. Refill the ring laser gyro with cleaning gas to the optimum coupling pressure specified for each gas.
4. Perform a dual discharge RF cleaning cycle for a 60-min period. Hold the ring laser gyro temperature rise to less than 350°F over this period.
5. Pump out cleaning gas, purge with He^4-Ne^{20} and evacuate overnight (approximately 15 hr).
6. Fill the ring laser gyro with He^3 and Ne^{20-22} in a 10 to 1 ratio to a pressure of six torr. Allow a 45-min mixing period.
7. Tip off the ring laser gyro from the fill station.

This processing schedule was considered to be the type of short-term procedure that would be practical with a successful RF cleaning cycle. Total cleaning and fill time is less than 24 hr.

After tip off each of the ring laser gyros was operated at a constant current value of 6 ma. Power output was monitored periodically with a Hewlett-Packard 8330A Radiant Flux Meter. Optical spectra were measured immediately after tip off and at selected intervals during the operating lifetime. The getters in each instrument were not fired so that impurity buildup with time could be monitored.

Figure 11 displays the power output curves taken during the operating lifetime of each of the ring laser gyros. One can note from the figure that the unit RF cleaned with oxygen exhibited the longest lasing lifetime of all. However, output intensity was not stable and decreased with time. Both of the units cleaned with the inert gases showed extremely short lasing lifetimes. The unit cleaned with nitrogen showed a power output dip with increasing lasing intensity until failure.

Examination of the optical spectrum of each of the life-test ring laser gyros shortly after tip off indicated a significant level of impurities in each unit. Both the argon and helium cleaned units showed considerable quantities of hydrogen (≈ 300 ppm) with no observable oxygen. The nitrogen-cleaned unit showed less than 100 ppm hydrogen present in the fill gas. The oxygen-cleaned unit showed nearly equal amounts of both oxygen and hydrogen with approximately 200 ppm of each gas.

Observation of the spectra at selected intervals during the lifetime period showed that the initial contamination levels measured in each ring laser gyro remained relatively constant for a period of time after which a rapid hydrogen buildup occurred. The hydrogen buildup in the oxygen-cleaned unit was somewhat slower than that in the other three. This can be seen in Figure 12, which is a plot of contamination increase with time for each of the life-test ring laser gyros.

It is interesting to note that for the units cleaned with the inert gases, the lasing action ceased long before the hydrogen buildup was observed in the tube.

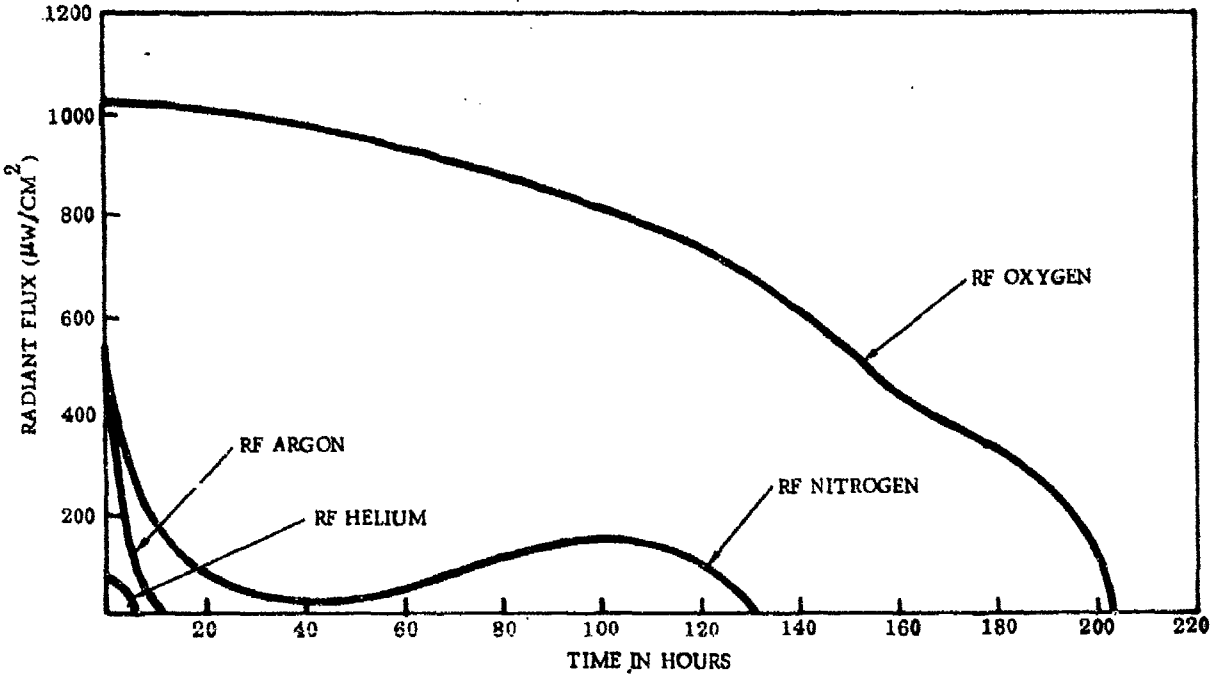

Figure 11. Power Output Curves During Life-Test of Ring Laser Gyros After RF Cleaning With Various Gases

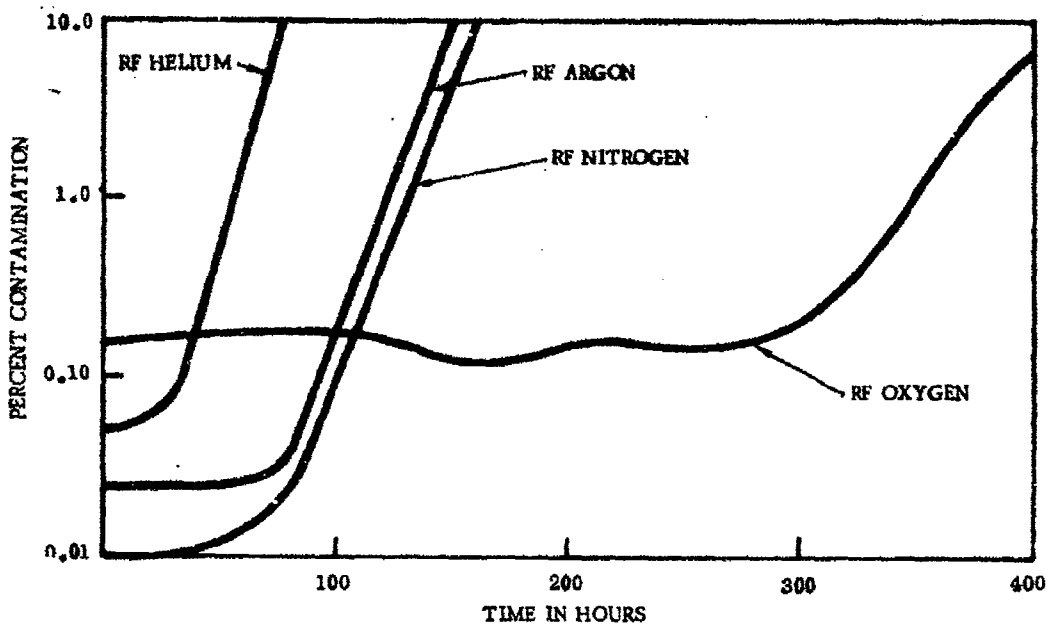

Figure 12. Contaminant Buildup With Time During Life-Test of Ring Laser Gyros After RF Cleaning With Various Gases

The steady state contamination level followed by rapid hydrogen buildup in each life-test instrument can probably be attributed to the gas clean-up action of the cathode. Initially, the pumping effect of the cathode is sufficient to handle the outgassing rate of the internal ring laser gyro surfaces. Saturation then occurs, and the cathode voltage drop increases with continuing impurity buildup, such that increased power is required to maintain constant plasma current levels. The increased power to the ring laser gyro possibly generates sufficient heat to rapidly liberate the pumped impurity materials from the cathode. Additional operation at constant current continually increases cathode heating due to continued impurity liberation. Gas clean-up effects were directly observed on the oxygen-cleaned ring laser gyro. The oxygen impurity level was observed to decrease from 200 ppm to ≈100 ppm during the lasing lifetime. The cathode design utilized for the 15-cm ring laser gyros has a surface area of 8.8 cm^2. Thus, at 4 ma it operates at a current density of 0.45 ma/cm^2. The rapid gas liberation effects at higher current densities may suggest that operating the cathode hotter at higher current levels would greatly reduce its gas clean up action.

Monitoring of the optical spectra also revealed a gradual buildup of the RF cleaning gas in the ring laser gyro during the life-test period. This was indicated in the unit cleaned with argon as a 25-30 ppm increase in argon concentration over a time interval of 140 hr. Similar impurity level increases of nitrogen were noted in the nitrogen cleaned ring laser gyro. Such liberation of cleaning gas suggests that it is being sorbed during the cleaning cycle. Also, ion implantation effects may be occurring due to the application of the high energy radio frequency field.

The life-test gas selection experiments indicate that oxygen is the most efficient and suitable gas for RF cleaning. The oxygen-cleaned ring laser gyro provided the highest intensity and longest duration lasing lifetime. Impurity degassing levels appeared to be significantly lower utilizing oxygen as opposed to other cleaning gases. Also, oxygen provides for the most efficient coupling of RF energy into the laser cavity so that maximum thermal degassing of the gyro surfaces can be achieved.

7. EFFECTS OF RF CLEANING ON RING LASER GYRO COMPONENTS

To assess the effects of the RF cleaning process on ring laser gyro components, a 15-cm instrument, similar to the ones used for the life-test portion of the program, was assembled and operated under maximum RF power and coupling conditions for over 20 hr. Temperature rise of the instrument was constantly monitored and kept below 350 F to ensure that adhesive bonds were not damaged by excessive heat. Prior to assembly, each of the components of the gyro was examined and characterized. The mirrors were photographed under 100X magnification as a reference for possible changes in scattering center density. After completion of the 20 hr test interval, subsequent disassembly and examination of the instrument indicated the following: (1) a very slight change in the surface structure of the fused-silica body in localized areas of the interior portion of the reservoir, and (2) a very faint deposit of metallic material near two of the getter pin feedthroughs. The surface structure change in the fused silica was probably due to breakdown of the material under RF field conditions. According to Bennett (Ref 1) neon atoms in the lower laser exacted state of a helium-neon plasma are de-excited by collision with the cavity surface. In this energy exchange the atom loses an energy equivalent to 16.62 eV. This energy loss to the surface is more than twice the energy required to rupture a silicon-to-oxygen and chemical bond (Ref 2). Studies by both Taylor (Ref 3) and Martinez (Ref 4) have also suggested that the interaction between the RF excited plasma and the cavity surface is a reduction process which is capable of decomposing silica to produce oxygen as a by product.

The metallic deposit noted in the gyro reservoir was traced to sputtering of the getter assembly. The sputtering appeared to be confined to the pin section alone and not to the getter trough. Gettering material was apparently unaffected and evaporated under normal firing conditions.

Examination of the mirrors after disassembly of the test ring laser gyro indicated no observable structural damage or increase in scattering center density. Breakdown or alteration of mirror surfaces will probably not occur with the dual DC-RF discharge cleaning technique since the RF field is not efficiently coupled into the bore sections. No coatings were observed on the mirror surfaces such as might have come from possible migration of decomposition products generated by RF field bombardment. This type of coating buildup seems unlikely, since sputtering is a ballistic rather than a thermal type process. The fact that the sputtering effects were noted in the gyro with time suggests that the RF cleaning technique could not be used for extended cleaning cycles at relatively high power levels such as 40 watts. Much lower power levels could be utilized for longer periods but would greatly limit the thermal degassing effects generated by the RF discharge. However, active cleaning should still be provided by electron and low energy particle bombardment. The use of lower power levels may also aid in reducing ion implantation effects.

8. NORMAL VERSUS RF PROCESSING

A 15-cm ring laser gyro designated RF-5, similar to the ones used for the gas selection studies, was assembled and processed utilizing normal thermal degassing techniques. This instrument was used as a reference point to compare the effectiveness of the RF cleaning process. The normal thermal degassing technique for ring laser gyros involves a four-to-five day processing cycle. The instrument is vacuum baked for a 50 to 60 hr period. Short DC oxygen discharge cycles are employed before and after baking as additional cleaning procedures. A 24-hr pump out is employed after final processing before the instrument is filled and tipped off.

Normal processing of the ring laser gyro was accomplished on a turbomolecular pumping station. The fill stand apparatus along with its attached thermal degassing chamber is shown in Figure 13. The normally processed 15-cm instrument was baked to a temperature of 280°F. This is somewhat below the baking limitation imposed by the epoxy sealing resin. The lower temperature was selected to insure that small leaks would not occur due to differential thermal expansion effects at the relatively large sized anodes employed on these gyros.

Power output and periodic optical spectra were measured during the life-test period. Figure 14 displays the output versus time for the normally processed gyro. The RF-oxygen cleaned gyro output curve has also been plotted in Figure 14 for comparative purposes. The laser output shows a more stable profile with time for the normal instrument. Laser lifetime is better by a factor of 1.2.

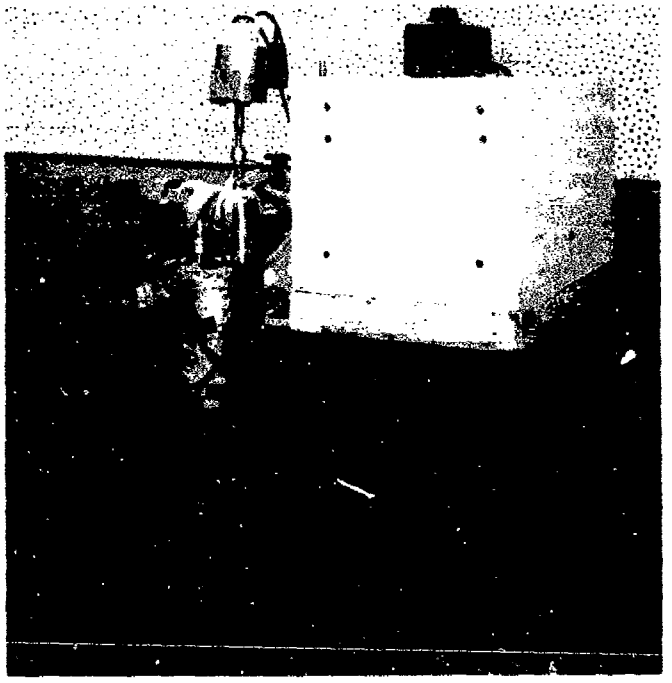

Figure 13. Fill Station for Ring Laser Gyros With a Turbomolecular Vacuum Pump and a Baking Chamber

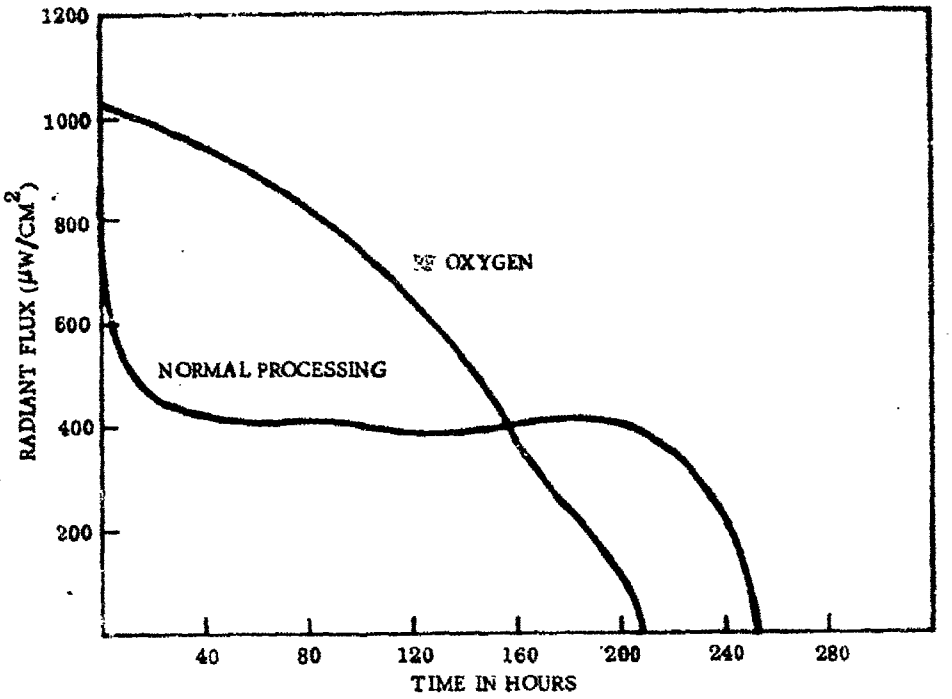

Figure 14. Laser Power as a Function of Time for a Normally Processed and an RF-Oxygen Cleaned 15-cm Ring Laser Gyro (Getters Not Fired)

The optical spectra of the thermally degassed ring laser gyro taken shortly after tip off indicated no detectable impurities. Observation of the spectra during the life-test interval showed virtually no impurity buildup for an extended period followed by an extremely rapid buildup of impurity which was substantially hydrogen. This is the same type of effect that was observed with the RF cleaned gyros and is no doubt due to gas clean-up effects. A dip followed by an increase in laser intensity can be noted in the normally processed gyro just prior to failure. The dip in intensity corresponded to a moderate increase in hydrogen. The following increase in intensity corresponded to rapid liberation of oxygen. Final quenching of laser action was due to very rapid hydrogen buildup which greatly attenuated the oxygen spectral transitions that had been observed earlier. The increase in power output corresponding to increased oxygen concentration certainly suggests that oxygen enhances laser action. Also cathode clean-up saturation effects appear to occur earlier for oxygen. This dip in power followed by an increase was also noted in the RF-nitrogen cleaned ring laser gyro.

Close examination of the optical spectra of the thermally degassed ring laser gyro indicated that after the very rapid buildup of hydrogen, the rate of hydrogen increase with time leveled off to a relatively constant value. This was also observed in each of the life-test gyros. This constant impurity increase with time may present a good indication of the actual hydrogen buildup rate of ring laser gyros. By utilizing the optical spectra data in conjunction with the impurity detection curves of Figures 7 and 8 the hydrogen buildup rates were calculated for each of the life-test instruments. Insufficient spectral data were available on the nitrogen-cleaned gyro for calculation. The calculated hydrogen rates are listed in Table I. One can observe that the rate is lowest for the normally processed instrument. The hydrogen buildup rate of the RF oxygen cleaned ring laser gyro is approximately twice that of the normally processed unit and is by far the lowest of the RF cleaned instruments.

Table I. Hydrogen Buildup Rates and Projected Lifetimes of Ring Laser Gyros

(Gyro) Cleaning Method	Hydrogen Buildup Rate (torr liters/sec)	Projected Lifetime (hrs/mg of getter)
(RF-1) Helium - RF	1.78×10^{-7}	47
(RF-2) Argon - RF	9.3×10^{-8}	89
(RF-3) Oxygen - RF	2.5×10^{-8}	334
(RF-5) Normal	1.23×10^{-8}	678

Impurity levels in a ring laser gyro must be kept at reasonably low levels to insure performance stability. This is normally accomplished through the use of gettering materials which effectively pump the contaminants which are constantly degassed from the wall of the instrument. The pumping rates of gettering materials have been fairly well established. If one knows the impurity buildup rates of a ring laser gyro, the total lifetime can be projected for a given amount of getter materials.

The projected lifetime per milligram of getter was calculated for each of the life-test ring laser gyros and is also listed in Table I. The calculation was made based on the assumption that both oxygen and hydrogen were primary contaminants in each gyro. The oxygen buildup rate was assumed to be equivalent to the measured hydrogen rate such that the total rate is twice that listed in Table I. The pumping rate of the gettering material was taken from the measurement of Ehrke and Slack (Ref 5). Their data show that a diffuse deposit of barium getter will pump approximately 60 liter-microns of hydrogen-oxygen gas per milligram of getter. The projected lifetime value for the normal instrument given in the table is in reasonable agreement (less than a factor of 2) with actual lifetime periods measured on ring laser gyros of similar configuration. All of the lifetest ring laser gyros employed two barium getters that each contained 4.4 mg of gettering material. Assuming approximately 80 percent of the available gettering material is successfully activated during firing, the total projected lifetime of each of the test gyros would be seven times the number calculated in Table I. Thus, the projected lifetime of a normally processed instrument would be slightly over 4600 hr.

9. NORMAL PLUS RF CLEANING

Two ring laser gyros were also processed to assess the possible cleaning improvements that could be realized by using the RF technique in addition to the normal thermal degassing procedure. The two gyros were processed simultaneously on the turbomolecular pumping station. One gyro, designated RF-6, was processed utilizing the normal baking procedure and was used as a reference for the experiment. The other gyro, RF-7, was processed in a similar fashion but in addition underwent an RF cleaning cycle. Figure 15 shows the arrangement for common attachment of the two ring laser gyros to the fill station. These two ring laser gyros were units that were previously processed during the RF gas selection experiments. The normally processed gyro was originally the unit employed for RF - helium cleaning. The normal plus RF gyro was originally the RF - argon cleaned unit. Both of these gyros originally showed very short lasing lifetimes. After failure each unit was opened to air for a two-day period before reattachment to the fill station. The RF cleaning cycle consisted of a 45-min dual DC-RF discharge period with oxygen. This was done

Figure 15. Normal Plus RF Cleaned Gyro and Reference Gyro on Fill Stand

both before and after thermal baking. The normal processed gyro employed similarly placed DC oxygen cleaning cycles. Pumping time after processing was 24 hr. Each gyro was filled to six torr with a ten-to-one mixture of He^3 and Ne^{20-22}.

Optical spectral taken on each ring laser gyro shortly after tip-off showed considerable amounts of oxygen impurity in both instruments. Under normal processing conditions a 24-hr pumpout is sufficient to remove all traces of oxygen from a ring laser gyro. Apparently, under RF-oxygen conditions sorption effects are greatly enhanced and desorption is a very slow process. Possibly some of the oxygen observed in the normally processed ring laser gyro is due to migration from the normal plus RF gyro. Also the fact that the two instruments were processed simultaneously may have presented additional gas conductance limitations for pumpout due to the manifold assembly.

Getters were fired in both of these instruments and comparative getter depletion rates were monitored. The getters should eliminate any cathode cleanup effects that might occur and establish equivalent impurity starting conditions so that degassing rates can be compared.

Removal of all observable impurities in the optical spectra of the normally processed RF-6 ring laser gyro occurred within minutes after the getter was fired. Removal of all oxygen impurities in the normal plus RF-oxygen processed RF-7 unit took 48 hr after getter firing. This suggests that continued desorption of oxygen was still occurring in this instrument with time.

The power output versus time of these two gyros is displayed in Figure 16. One can note relatively stable operation through the lifetest period to date. The slight variations in intensity are probably related to multimode conditions since these instruments were not apertured. As of 9 March both instruments had been operational for over 646 hr. The comparative depletion rates of the getters in each instrument were observed to be greatly different for the first 100 hr of operation in that the depletion of the normally plus RF cleaned gyro was nearly twice that of the normally processed unit, suggesting oxygen desorption was still continuing. During the last 100 hr of operation, depletion rates have been noted to be nearly the same. It appears that getter depletion rate will have to be monitored over longer time periods to assess possible improvements in degassing rates.

After 430 hr the getter on the normally processed gyro had been depleted by approximately 20 percent from its initial volume. If the gyro continued to deplete getter at this rate its total lifetime would be approximately 4300 hr. This is in good agreement with the projected lifetime calculated for gyro RF-5 in Section II-6. Additional data were obtained on a 40-cm ring laser gyro as to the effects of normal processing plus RF cleaning. The gyro was cleaned utilizing the normal vacuum degassing cycle of 300 F for 48 hr. After completion of all processing steps the instrument was filled with helium-neon gas and was observed to lase with nominal intensity. Subsequent RF cleaning utilizing the same helium-neon fill mixture liberated sufficient contaminant gas to reduce laser intensity by a factor of four.

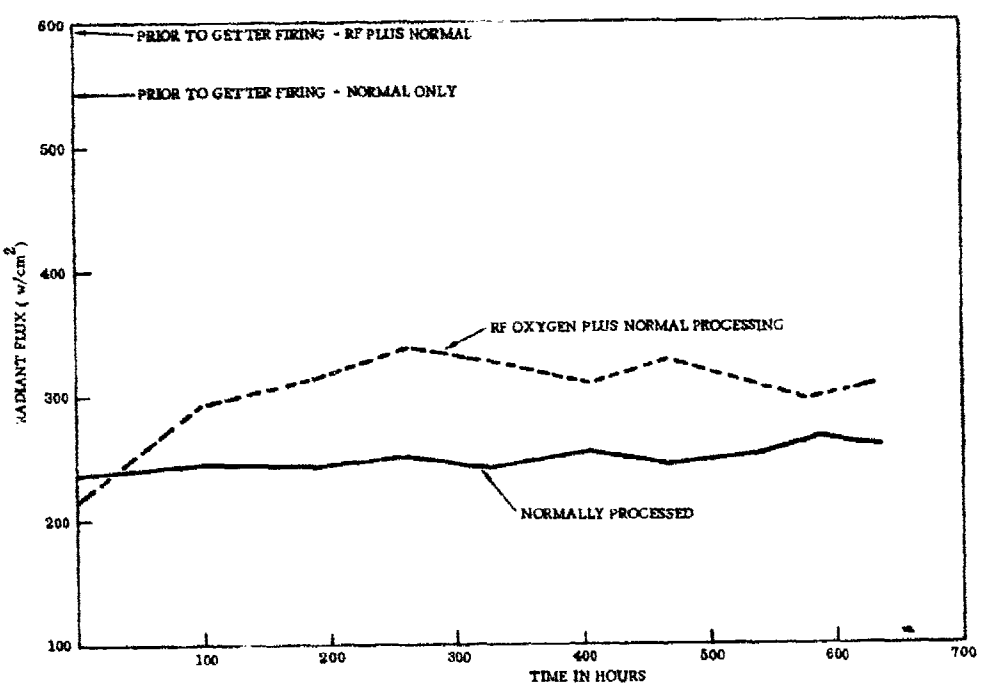

Figure 16. Power Output vs Time for Ring Laser Gyro RF-6 (Normal Processing) and RF-7 (Normal + RF Oxygen) After Getter Firing

10. CONCLUSIONS AND RECOMMENDATIONS

The specific conclusions derived from the RF cleaning studies were as follows:

1. Although the RF cleaning process is a feasible and effective technique for ridding ring laser gyros of contaminants, it does not alone provide for the levels of cavity cleanliness that can be achieved with thermal degassing procedures. However, RF cleaning used in conjunction with vacuum baking can produce cleaner cavities than can be obtained by using only thermal processes. Thus, it is recommended that an RF cleaning cycle be added to all ring laser gyro processing techniques.

2. The primary cleaning improvement provided by the RF process is its ability to liberate impurities from the reservoir section of the gyro. With conventional processing any cleaning effects from plasma bombardment are confined to the bore and cathode section which constitute only a small portion of the gyro surfaces. With the RF cleaning process, plasma bombardment occurs at all the interior surfaces of the gyro.

3. Oxygen provides the most efficient gas medium for the RF cleaning process at optimum coupling pressure. However, oxygen because of its reactive nature readily enters into sorption-desorption interaction and is removed very slowly from the gyro. Thus, RF processing should be performed prior to thermal degassing procedures which will facilitate oxygen removal.

4. Extended RF coupling into a ring laser gyro can cause sputtering of gyro components. Therefore, the RF cleaning cycles should be confined to moderate power levels of less than 25 watts and to short time intervals of less than 45 min.

5. A dual DC-RF discharge technique provides the optimum coupling mechanism for RF cleaning. The gain section of the ring laser gyro is weakly coupled so that lower energy bombardment effects occur to clean without damaging optical surfaces. The reservoir section of ring laser gyros couple very efficiently and higher energy impingement occurs to accelerate cleaning effects.

6. Because of the possibility of sputtering and implantation effects under energetic RF conditions the RF process cannot be used for extended thermal degassing.

7. Small amounts of oxygen enhance 1.15μ laser output power. Small amounts of hydrogen greatly reduce laser output.

8. Optical spectroscopy is a useful technique for determination of impurity buildup under operational conditions. However, it is difficult to distinguish types of contaminants and quantitative amounts from optical spectra. Also, analysis of multiple impurities is difficult due to attenuation effects.

Future work to reduce contamination levels in ring laser gyros should probably involve the measurement of outgassing rates for each of the identifiable impurities in the gyro. With this knowledge thermal degassing times and temperatures can be established along with RF cleaning procedures to reduce gyro outgas levels to sufficiently low rates. Techniques also need to be established for precise monitoring of gyro contamination levels while both on and off the gas fill station. Mass spectrographic analysis used in conjunction with a multichannel optical spectrum analyzer which observes transitions from the ultraviolet to the infrared may provide the most precise monitoring techniques. and valuable information of the plasma chemistry of the helium-neon discharge.

Future work also needs to be done to better establish the exact effects of gas contamination on ring laser gyro performance.

SECTION III

RING LASER GYRO FABRICATION

1. INTRODUCTION

In this section the ring laser gyro fabricated by Autonetics for AFAL is described. The unit contains a ring laser gyro angular sensor and all required power and control electronics suitably packaged for laboratory tests at Holloman AFB.

The ring laser gyro instrument has been designated RLG-1140. It contains the latest Autonetics state-of-the-art refinements to a design which has been highly developed, built up into hardware, and tested previously. The RLG-1140 exhibits the good bias stability and linearity characteristics of the previous Autonetics 40-cm ring laser gyros. In addition, modifications have been made in mounting design, thermal design, magnetic design, and fill stand processing which significantly improve other areas of performance. Instrument temperature sensitivity is reduced through the use of a thermal control structure which surrounds the instrument on all sides and shields it from ambient disturbances as well as permitting rapid temperature control. The magnetic design improves bias repeatability through the removal of all materials which retain significant residual magnetization from close proximity to the Faraday bias package. Lifetime is extended through the use of RF cleaning techniques along with the utilization of a long-term vacuum bake in the fill stand processing.

The electronics for RLG-1140 consist solely of proven circuitry functions which provide complete sensor control, including Faraday biasing, all secondary voltages and controls, and rapid output data processing. These electronics are of a modular design which facilitates maintainability of the package. The electronic unit is adaptable to the control of additional ring laser gyros with certain modifications.

The organization of the following material is as follows. First, the features of the instrument and electronic design are discussed. Operating procedures and electronic design are discussed. Operating procedures and electronic schematics are included. Next, a summary of test data collected at Autonetics with RLG-1140 is presented. This part of the report concludes with a discussion of reliability, maintainability and system safety considerations made for ring laser gyros.

2. RING LASER GYRO DESCRIPTION

The RLG-1140 instrument is the third iteration in a 40-cm pathlength design originally developed for AFAL under Contract F33615-70-C-1618. The basic features of the RLG-1140 design are as follows:

Size: Volume	43 in.^{3}
Width	6.5 in.
Weight - Sensor	2.6 lb
Pathlength (geometric)	40.5 cm
Scale Factor	1.7 $\widehat{\text{sec}}$/pulse
Bore Size	0.080 in.

Gas mixture	9:1 He^3:Ne Total pressure = 3.3 torr
Excitation voltage	1150 volts
Discharge current (total)	4 ma
Wavelength	0.633μ
Laser frame material	Ultra-Low Expansion (ULE) titanium silicate
Readout Device	Dual silicon photodiode
Antilock mechanization	Faraday bias package

In Figure 17 a full-size drawing of RLG-1140 is shown. The basic ring laser gyro concept developed by Autonetics utilizes a precision triangular optical cavity in an integral ultra-low thermal expansion body. The pathlength of 40.5 cm is the largest possible commensurate with single axial mode operation. (Performance improves with increase in cavity length.) The instrument is constructed of ULE titanium silicate and has a 0.080-in.-diameter bore along each of the legs of the triangle to form the optical path. The center of the body is hollow to provide for a gas reservoir and to accommodate a cathode and getters. At the three corners of the triangle, high-quality reflectors are bonded.

Gyro output nonlinearities are minimized through implementation of a proprietary multiple FM biasing technique via a Faraday bias element in one leg of the triangular optical path. With this type of bias scheme output nonlinearities are removed through application of an AC electrical signal rather than with any mechanical motion, resulting in no moving parts and inherently higher g capability. The detection of the magnitude and the sense of the gyro beat frequency is achieved through the use of a dual photodiode mounted adjacent to a combining optics prism on the output mirror.

In the following paragraphs the crucial design features of RLG-1140 are discussed in detail.

a. Body Material

In order to minimize thermal effects, ULE titanium silicate was chosen as the body material. This material has a thermal expansion coefficient of 3×10^{-8}/deg C. With this material warm-up time can be minimized. Angular tolerances are selected to allow easy fabrication and optical alignment.

b. Bonding Cement

The cement used on parts which have access to the plasma section of the instrument is an anhydride-cured filled epoxy which is bakeable to 300°F. Important features of this cement include: low water vapor transmissibility, constant long-term adhesive and chemical properties, low resin creep on polished surfaces, and compatible thermal expansion.

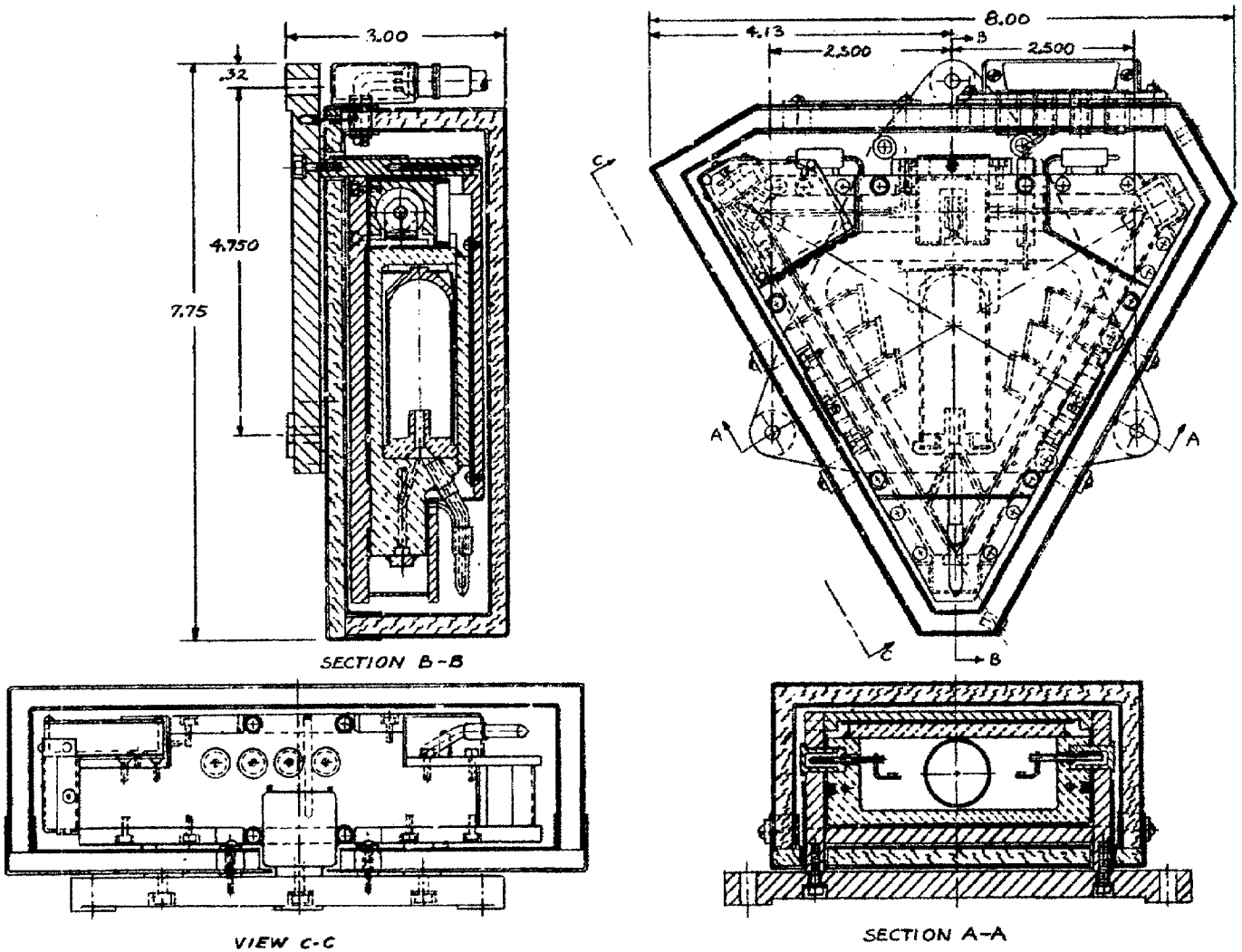

Figure 17. Ring Laser Gyro Assembly

c. Laser Wavelength

For several reasons, including the laser linewidth and input power requirements, a helium-neon mixture was chosen as the lasing medium. The 0.633-μ visible transition in the He-Ne system was chosen for the operating wavelength in preference to the 1.15μ IR transition possible in the same gas system. This choice was made because both theoretical and experimental studies indicate that performance at 0.633μ would be superior to that in the IR.

d. Bore Size

In the design of the optical cavity, the bore size must be considered along with the mirror radii in determining such quantities as laser gain, fabrication tolerances, and alignment tolerances. From the point of view of gain, smaller bore size is favored, because gain per length is inversely proportional to bore diameter. However, smaller bore size reduces the tolerance allowable in placing mirrors and windows onto the gyro body and also causes diffraction losses if made too small compared to the spot size of the laser beam. For these reasons a compromise must be reached. This trade-off resulted in the choice of a 0.080-in. bore size. This bore size was easily drilled into the ULE block. It permits gain per length of the instrument to be greater than 0.1 percent/cm, which is quite adequate for good operation.

e. Choice of Polarization

The orientation of the Brewster-angle windows which terminate the plasma section of one leg of the instrument, fixes the polarization of the two counterrotating laser waves to be s-polarization. This polarization is desirable because ultra-high reflectivity mirrors are easier to obtain for s-polarization than for p-polarization with light incident on the mirrors at 30 deg, as in the case of RLG-1140.

f. Mirrors

Three multilayer dielectric mirrors are used to terminate the optical cavity. Two of the mirrors have ultra-high reflectivity (~0.05-percent transmission loss). The third is an output mirror with 0.4-percent transmission at 30 deg angle of incidence. One of the ultra-high reflectivity mirrors is deposited on the flat surface of a specially prepared diaphragm substrate which is backed by a piezoelectric element to control the optical pathlength. The second ultra-high reflectivity mirror is deposited on a curved substrate. The mirror radius chosen produces a relatively small spot size at the surface of this curved mirror, which is the point of maximum beam size in the cavity. With this spot size, body fabrication tolerances were routinely met, and optical alignment was assured when the gyro was assembled. The third mirror, or output mirror, is a flat mirror. An additional requirement on this mirror is that its front and back surfaces be parallel within a few seconds of arc so that the combining-optics prism mounted on it will function properly.

g. Combining-Optics Prism

A combining-optics prism is mounted on the output mirror to make the counter-rotating-beam outputs nearly collinear before they impinge on a photodetector. The angle between the two beams just after exiting from the combining-optics prism is

given by 2nθ. In this expression, n is the index of refraction of the prism material and θ is the amount by which the prism corner angle deviates from 90 deg. The angle 2nθ is typically about 1.5 min, and it determines the regions in which the two beams interfere constructively and destructively, i.e., the fringe spacing. The prism corner angle in this case was chosen so that the two detectors spaced a certain distance apart in a standard dual photodiode package are spaced 90 deg apart on the fringe pattern. Two detectors positioned in this way yield sense information as well as magnitude information.

h. Cathode

A cylindrical aluminum cathode with specially prepared oxide-coated surface is employed in RLG-1140. Because of the large cathode surface area, the cathode current density may be maintained at a low value. Sputtering and subsequent gas cleanup will be inhibited due to operation at this low current density. This design is the result of an intensive research program that included consideration of material properties which relate to outgassing, sputtering, and ionic pumping and discharge properties dependent on current density through size, shape, and discharge geometry.

i. Anodes

Two glass-beaded Kovar anodes are used on the instrument. Each anode terminates a gain section of equal geometric length within fabrication tolerance and equal discharge current within 0.1 μa. With current paths balanced in this way, Langmuir flow bias effects are minimized.

j. Getters

Six barium-aluminum alloy getters are mounted in the gyro gas reservoir. Each getter bar contained 4.4 mg of getter material. The getters were fired under vacuum prior to final gas fill on the fill stand.

k. Apertures

Aperture parts are mounted on ULE spacer blocks in the gap between the Brewster-angle windows. The aperture comprises two rods with highly polished ends mounted orthogonally on the spacer blocks. One rod is the aperture in the x direction and the other in the y direction. The opposite end from the polished end on each rod is threaded, so that the aperture rod can be held in place by a locknut once it is properly adjusted. Aperture rods are adjusted so that TEM_{00q} modes oscillate in the RLG while transverse off-axis modes experience too much loss to lase. The aperture rod material was chosen to be Mallory metal, a low thermal coefficient of expansion metal.

l. Gas Fill Mixture

The laser gain medium is a helium-neon gas mixture. From previous studies at Autonetics, it was known that a certain ratio of Ne^{20} to Ne^{22} yields best gyro performance. This optimum ratio was used in filling RLG-1140. The He:Ne ratio and total pressure are slightly higher than the optimum values for the operating current desired (4 ± 2 ma). As tube gas pressure decreases with time due to helium diffusion and gas cleanup, tube gain should increase slightly before decreasing. This will tend to make gain more level with time initially. The tube design is such that helium diffusion should not cause significant tube operational degradation for a period of several years.

m. Pathlength

In general, larger ring lasers exhibit better performance than smaller ones, in agreement with theory. Larger instruments also have larger scale factors. For fixed bore size, a longer tube has higher gain than a short one and will lase even with higher losses in its optical circuit. For these reasons, it is desirable to build a ring laser gyro with the longest pathlength compatible with single axial mode operation. This pathlength is approximately 40 cm.

n. Magnetic Shielding

Multiple magnetic shields are employed in order to reduce RLG sensitivity to stray magnetic fields. First, the most field-sensitive quantity in the instrument, the Faraday bias package, is surrounded by a molypermalloy shield. The entire instrument assembly is then enclosed by two outer molypermalloy magnetic shields separated from one another by 1/4 in. of insulation.

o. Photodetectors

A standard silicon dual photodiode package containing two detectors mounted a small distance apart is adjacent to the combining-optics prism. The spacing is such that the detectors can be adjusted to be 90 deg apart on the gyro output fringe pattern. Two detectors positioned in this way yield rotational sense information as well as magnitude information. The detectors chosen and preamp design employed permit a dynamic range in excess of ±100 deg/sec to be realized.

p. Frequency Lock Prevention

A Faraday bias package is used in RLG-1140 in order to linearize the gyro input-output curve. The physical location of the bias package is in one leg of the RLG between the two Brewster-angle windows. The manner in which the Faraday package introduces a bias can be understood from consideration of the following information.

When plane-polarized light traverses an optical medium along the direction of a magnetic field, the plane of vibration is rotated. The sense of rotation is reversed if the direction of the magnetic field is reversed. The angle of rotation depends on the optical material and is proportional to the magnetic field strength and the length of path in the medium. This phenomenon is called the Faraday effect.

In the ring laser, a Faraday material is combined with two quarter-wave plates, one at each end of the cell, to generate an artificial bias. The quarter-wave plates are oriented with their slow and fast axes, respectively, aligned so the net phase change for light traversing both of them is zero when no magnetic field is applied. The light in the ring laser is plane polarized (s-polarization) due to reflection losses of p-polarized light from the windows oriented at Brewster's angle with respect to the direction of light propagation. For maximum bias scale factor, the plane-polarized oppositely directed traveling waves are changed to circularly polarized light before entering the cell by orienting the quarter-wave plate axes at 45 deg to the direction of light polarization. Both waves have the same sense of polarization but traverse the cell in opposite directions. The magnetic field is in a different direction for each wave. As a result, one beam is advanced in phase while the other is retarded. The two traveling waves are converted back to plane-polarized light by the second quarter-wave plate. The phase shift results in a frequency difference between the traveling waves.

The scale factor of the package in RLG-1140 is given by:

$$\frac{B}{H} = \frac{c\, V \ell_1}{1.08 \times 10^4\, L}$$

where

$\frac{B}{H}$ = scale factor (Hz/gauss)

c = velocity of light = 3×10^{10} cm/sec

V = Verdet constant of Faraday material ($\widehat{\text{min}}$/gauss-cm)

(V = 0.147 for glass used in RLG-1140)

ℓ_1 = length of Faraday element (cm) = 0.38 cm

L = optical perimeter of ring cavity (cm) = 40.9 cm

With parameters appropriate for RLG-1140, the scale-factor B/H is found to be 3800 Hz/gauss.

The bias package in RLG-1140 is made up with a 0.38-cm-long glass Faraday element and two 1-mm-thick quarter-wave plates. The package is bonded together with an optical cement whose refractive index is intermediate between the indices of the Faraday element and the quarter-wave plates. The outer surfaces of the quarter-wave plates are antireflection-coated to prevent reflection losses upon insertion in the RLG. The bias package is mounted in a beryllia holder which in turn is mounted to a reference surface on the gyro body.

The use of beryllia facilitates rapid temperature control of the Faraday package. By employing the heater-sensor mounted directly on the beryllia part, the Faraday bias package can be brought up to its operating temperature within less than two minutes and held fixed to better than ±0.1°F. The field coils which are used to apply an ac magnetic field to the bias package are contained in an aluminum housing which slips over the bias package. The aluminum housing in turn is contained in a molypermalloy magnetic shield which is connected directly to the gyro base plate. In this way, heat developed in the field coils can be shunted to the gyro base. Two coils mounted coaxially with the bias package (one on each side of the package) are used to apply the ac bias fields. Each of the coils has two windings.

The method employed for reducing frequency-locking effects to tolerable limits is the electronic FM-bias technique. Effectively an electronic dither signal, the FM-bias signal is applied through an electro-optical device (Faraday element) so that the RLG signal is rapidly driven through the input rate range where it tends to lock. The result is a linearized input-output characteristic which provides good performance over a wide input rate range including zero rate.

Several FM bias schemes have been conceived, analyzed, and tested in operational form at Autonetics. All schemes can be described by the following generalized differential equation for the locking dynamics:

$$\frac{1}{2\pi}\dot{\psi} = B_O + B_L \sin \psi + \sum_i B_i g_i(t)$$

where

ψ = heterodyne signal phase

$\dot{\psi}$ = $\frac{d}{dt}(\psi)$

B_O = angular rate to be measured

B_L = locking threshold

B_i = modulation depth of i^{th} FM bias signal (amplitude of the signal)

$g_i(t)$ = unity amplitude time function of i^{th} FM bias signal.

The average value of $\frac{\dot{\psi}}{2\pi}$ is the analog of the input rate, B_O. The locking threshold, B_L, describes the width of the dead zone occurring about zero input when no bias scheme is used. The FM bias signal itself can be either a single waveform or a combination of two or more waveforms. Achievement of optimum performance is critically dependent upon selection of FM bias signal parameters.

A multiple FM bias scheme is implemented in RLG-1140. Several ac bias waveforms are summed and applied to the Faraday bias coil. The rates and depths of the waveforms are chosen from a computer simulation of the RLG equations with FM bias in order to reduce nonlinearities to less than 0.025 percent. Total bias package power is an optimum value compatible with bias package thermal design.

q. Thermal Control

There are two temperature-control circuits operative in the RLG-1140. One controls the Faraday bias package temperature and the other the overall body temperature.

A heater and sensor are mounted directly on the beryllia holder for the Faraday bias element. With this arrangement, the bias package can be brought up to its operating temperature within less than 2 min and held there to better than $\pm 0.1^{\circ}F$. The control temperature is typically a few degrees higher than the overall body temperature. It is important to hold the bias package temperature fixed, because modulation index settings are critical and must be maintained. Modulation index values will vary with temperature due to change in bias package scale factor with temperature.

The ULE body is enclosed on all sides as well as top and bottom with a high heat transfer structure which consists of a thin beryllium copper sheet held against the body by a corrugated beryllium copper sheet spring captured within a thicker aluminum sheet which is the principal thermal conductor, Figure 18. The ULE body is held under slight spring compression on all surfaces from the heat transfer structure and is in positive contact for location with three raised pads on the thick aluminum bottom conductor sheet. The heat transfer structure which contains the ULE body is supported by three mounts located at the middle of each side. The mounts extend below the bottom of the heat transfer structure and bolt to the RLG base plate. Each mount contains a thermistor and has a heater element attached to the outer surface for steady state temperature control of the RLG. The principal thermal paths out of the heat transfer structure are through the three mounts to the base plate.

r. Cavity Length Control

Due to small optical length changes in the ULE body, the fused-silica Brewster angle windows, and the piezoelectric package during warmup, cavity length is maintained constant by varying the voltage applied to the piezoelectric package. The piezoelectric package employed produces a one wavelength (one mode) shift per 80 V applied. Such a large swing at such a comparatively low voltage is achieved by cementing together many 0.010-in.-thick plates and connecting all of these in parallel electrically. Assembly of the package with very thin cement layers produces a piezoelectric stack with a thermal expansion coefficient comparable to the fused silica housing which contains it.

3. ELECTRONIC DESIGN

The RLG control electronics provides laser optical path length control, plasma starter logic, active plasma discharge current balance, Faraday bias and bias heater control, and photodetector readout electronics. Figure 19 shows a functional block of the RLG and Electronics.

a. Interface Description

(1) Input Power Requirements

Input power shall be +28 ± 2 VDC with a peak requirement of 50 watts during normal operation.

(2) Output Signals

There are two output data lines for RLG output data. The instrument output consists of an A and B output line in A-B format. The output levels are compatible with standard TTL logic input requirements. The output waveform is shown in Figure 20 and is a fixed pulse of 0.5 μsec width with a scale factor of 1 pulse per 1.7 sec rotation.

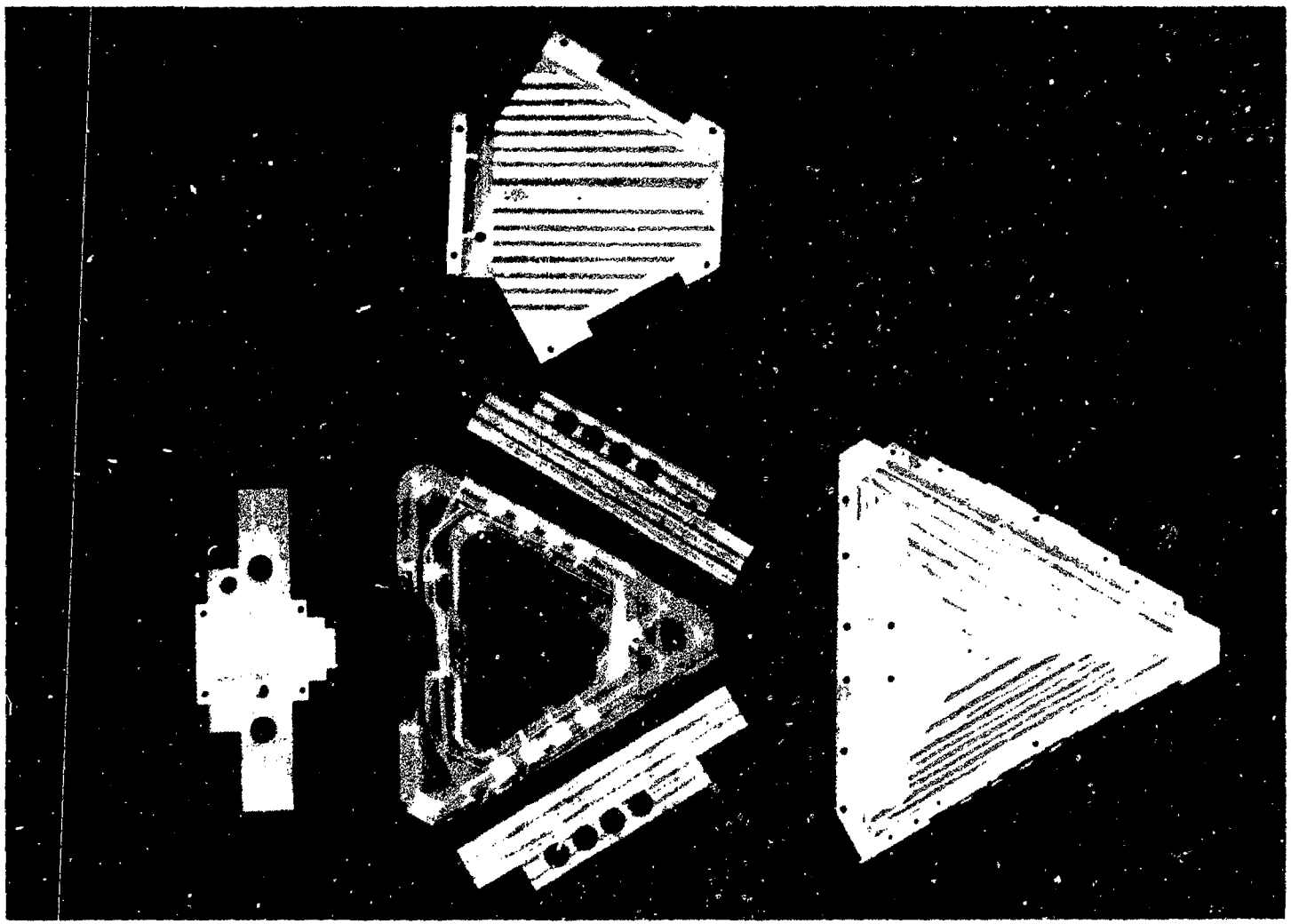

Figure 18. Ring Laser Gyro Body and Thermal Control Structure

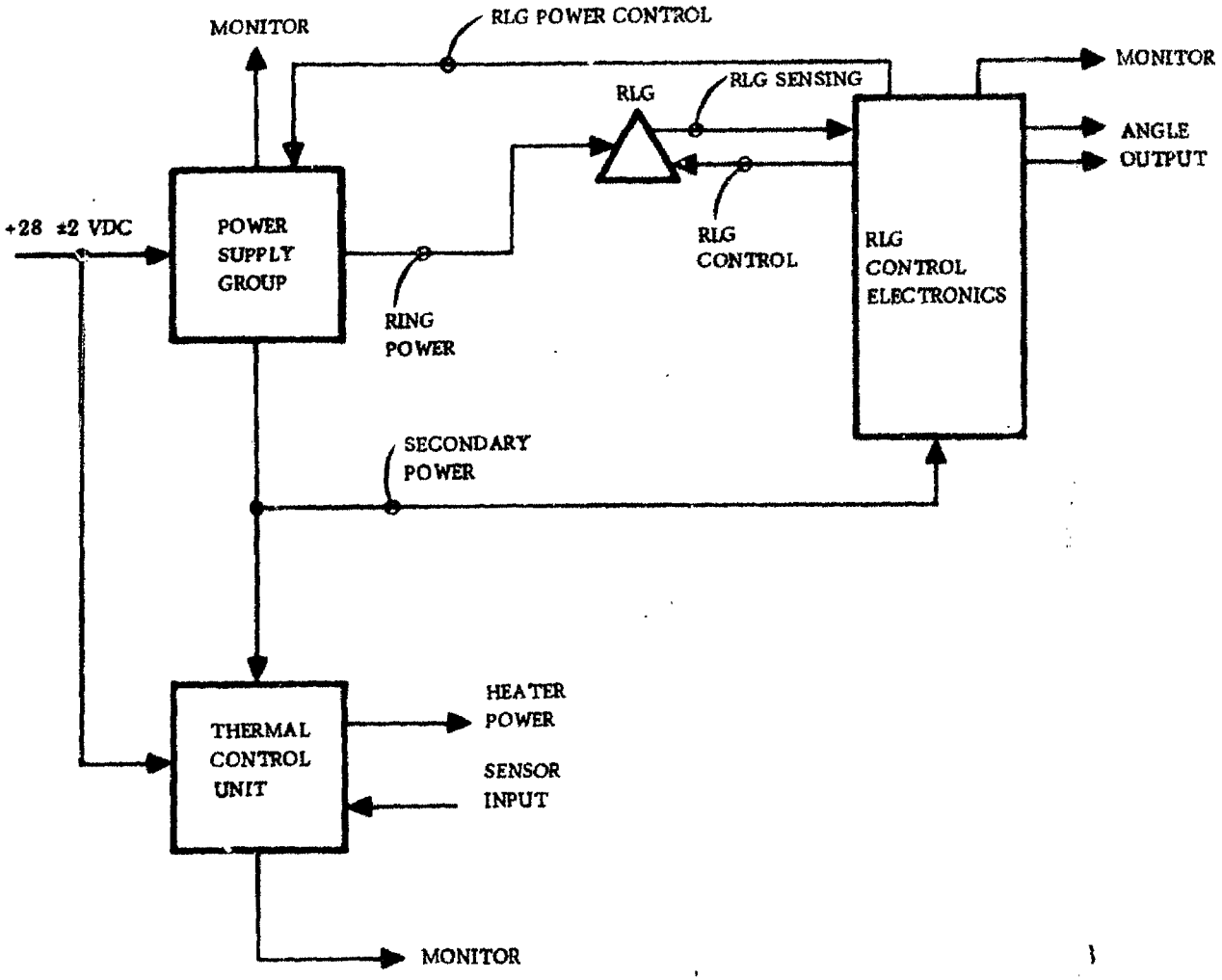

Figure 19. Ring Laser Gyro Model RLG-1140 and Electronic Controller Model 717 Functional Block Diagram

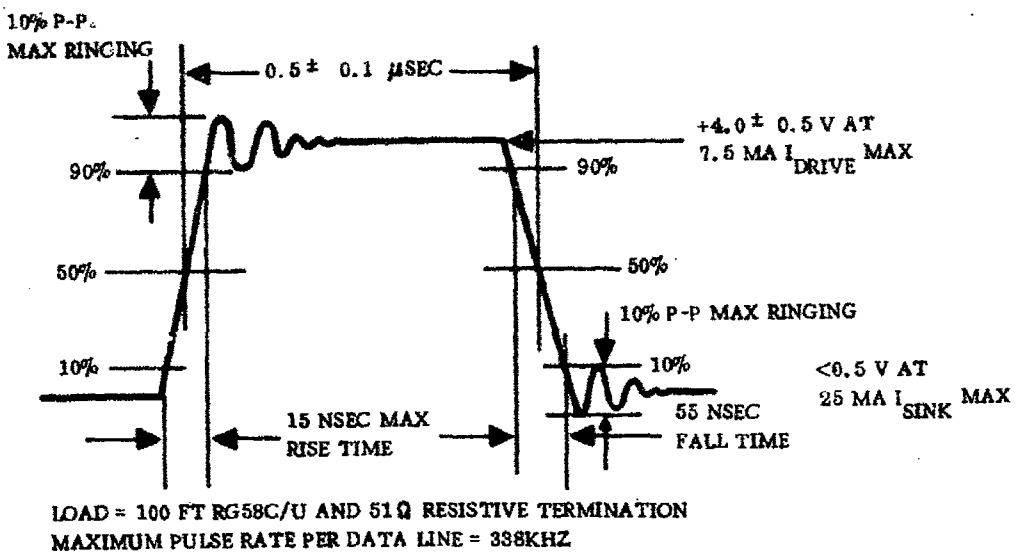

Figure 20. Ring Laser Gyro Data Line Waveform

The load condition imposed on each output driver is dependent on the length of coaxial cable attached and the number of TTL devices to be driven. The following criteria shall be used.

1. A maximum of 100 ft of RG58A/U or equivalent (29 pfd/ft) shall be used on each line.

2. Any pair of data lines shall be of equal length. If lines are in excess of 15 ft in length, then a 50 ohm ± 10 percent resistance termination will be required. A maximum of five TTL devices will be used to terminate each line.

b. Detailed Functional Description

(1) Power Supply Group

(a) EMI Filter, Reverse Polarity and Transient Protection Circuit. An EMI filter is used in the primary power +28 VDC and return lines to prevent any noise on the power supply from reaching the electronics. It also prevents any EMI generated in the switching preregulator from getting out of the electronics back into the power supply. A diode is connected in series with the +28 VDC input to protect against accidental reversals of input power polarity. A Thyristor diode is placed in shunt with the input power and is set to conduct at 36 to 38 V. A fuse in series with the +28 V will open circuit if an overvoltage condition occurs.

(b) Switching Preregulator and Circuit Breaker. A power switching transistor, commutating choke, and an IC voltage regulator comprise the switching preregulator and circuit breaker. This circuit provides two functions: (1) It has a wide input voltage range and provides a very efficient means of stepping down a high AC voltage to a lower constant DC voltage, and (2) the addition of two small signal transistors Q2 and Q3 across a current sampling resistor make the regulator IC and power switching transistor Q1 function like a circuit breaker. The circuit breaker is set to act if the load current exceeds 4.5A. To reset the circuit breaker, simply remove the +28 V input for a 5 sec period and then reapply power. If overload has cleared, then the breaker will be reset, and all will operate normally. A measured efficiency of this circuit under normal operating conditions is between 90 and 95 percent depending on input voltage and load current. The switching frequency is provided by the low voltage DC-to-DC converter stage. This prevents any tendency for the switching regulator and inverter to "hunt" or drift across each other's frequency, which can cause large low frequency ripple to appear on all DC outputs from the low and high voltage supplies.

(c) Low Voltage DC-to-DC Converter. This module is used to provide all voltage levels used in the control electronics group and regulated +28 VDC to the Faraday dither generator power amplifier. The inverter stage is a saturating flux oscillator which runs at approximately 18 kHz switching frequency. A special alloy 0.5 mil tape toroid core is used in the transformer in order to keep switching losses down and improve transformer regulation. A toroid core is used to provide minimum stray field radiation as well as best efficiency. All secondary voltages are provided with an independent winding for each. Each secondary winding is optimized for wire size in accordance with the load current required. Each winding is followed by a full wave capacitor input rectifier-filter system. Ferrite beads are used in all areas where transient suppression is of importance. These little devices make an ordinary conductor into an RF choke and thus present a high impedance to transient currents. Close attention is paid to the power returns or grounds. This is the major advantage to individual secondary windings in that common ground currents can be eliminated. Both +15 V and -15 V tracking voltage regulators are provided to ensure complete immunity to any input voltage fluctuations for all precision circuitry and references. The +15 V and -15 V regulators are also used as circuit breakers to protect the precision circuitry should a short or overload occur during maintenance or setup procedures. This feature was considered necessary because the power dissipation of the regulators could be easily exceeded if such a fault condition occurred. About 20 times normal load currents would be required to cause the main circuit breaker to function. The +15 V and -15 V regulator/circuit breakers are interlocked so that an overload on either will shut down both sides. To reset the circuit breakers, follow the same procedure as mentioned previously for the switching regulator - main circuit breaker reset operation.

(d) High Voltage DC-to-DC Converter, Electronic Ripple Filter, and Voltage Regulator. This module provides the DC excitation power for the RLG plasma. It is designed to operate one 40-cm RLG at a total continuous load of 7 ma at -1500 VDC output. The inverter stage is a saturating flux oscillator. The secondary transformer voltage is 750 VAC. This is full wave voltage doubled and run through a three stage RC filter to remove harmonics and reduce the ripple at full load to about 2 V p-p. Voltage regulation is achieved by a switching regulator in the +28 VDC input circuit. The control signal is derived from the anode current source circuit and serves to keep the voltage drop across the current source control transistors constant at around 75 to 100 VDC.

(2) RLG Control Electronics

(a) Path Length Controller. The block diagram of the pathlength control electronics is shown in Figure 21. The cavity length is modulated at a low audio-frequency rate by driving a piezoelectric transducer with a 1-kHz sinewave signal. This produces a corresponding modulation of the output intensity to the photodetector. When the cavity length is located at the center of the intensity curve, the output power is modulated at twice the fundamental frequency. The output will be either in phase or out of phase with the driving frequency, depending upon whether the pathlength is longer or shorter than that which maximizes intensity. Thus, by demodulating the 1-kHz pickoff signal at the photodetector and servo-controlling the cavity length to produce a null signal, the cavity length is stabilized.

The pathlength control electronics consist of two active 1-kHz bandpass filters, a demodulator, an integrator, a 1-kHz oscillator (part of the signal generator module), and a high-voltage amplifier. The bandpass filters are centered at 1-kHz and provide the required signal-to-noise at the demodulator input. The integrator provides a high gain at dc, which provides an average pathlength control error of less than 0.02 μin.

(b) Data Converter. Refer to Figure 22 for the functional flow of the readout signals. Power modulation of the laser beam is converted to current modulation with a dual, high-speed silicon photodiode, which is spaced to provide two quadrature signals with an integrated circuit operational amplifier. The sinewave outputs of the amplifier are converted to two square waves in quadrature. Logic is performed on the signals to determine the quadrature phase relationship (rate direction) and convert the signal frequency to pulse rate (rate magnitude). Pulse transformer coupled outputs can be provided to give complete ground isolation if so desired.

(c) Current Source and Starter. Figure 23 shows the plasma excitation block diagram. An active current source is utilized in series with each anode to provide dynamic high frequency response to any change in anode current. A single temperature compensated zener source is the precision reference for both anode circuits. In addition, the individual current sources are coupled with an active current balance circuit which provides further anode current stability as well as maintaining the anode currents equal within 0.1 μamp. Thus, balanced anode currents are obtained regardless of changing conditions at the plasma tube, such as anode resistance, dynamic gas characteristics, etc. A logic network continuously monitors the individual current sources and activates or turns off the high voltage starter pulses which induce the ring plasma discharge ignition as required. A 1-kHz pulse signal from the cavity length control reference oscillator when applied to the starter circuit results in a 4000 V high frequency pulse of 1 msec repetition rate applied to the gyro. This pulse easily initiates the gas discharge which is sustained by the high voltage supply and the current sources.

A signal output is provided to the high voltage supply as reference to cut back its output when the gas has ionized and the current sources are operating nominally.

(d) Thermal Control. Temperature control is provided for the RLG by a set of thermistors and heaters mounted in the instrument. The controller is referenced to a temperature-compensated zener source and provides control of the constant temperature supports for RLG thermal control structure to approximately 0.05 F. This condition can be maintained between 75°F and 85°F.

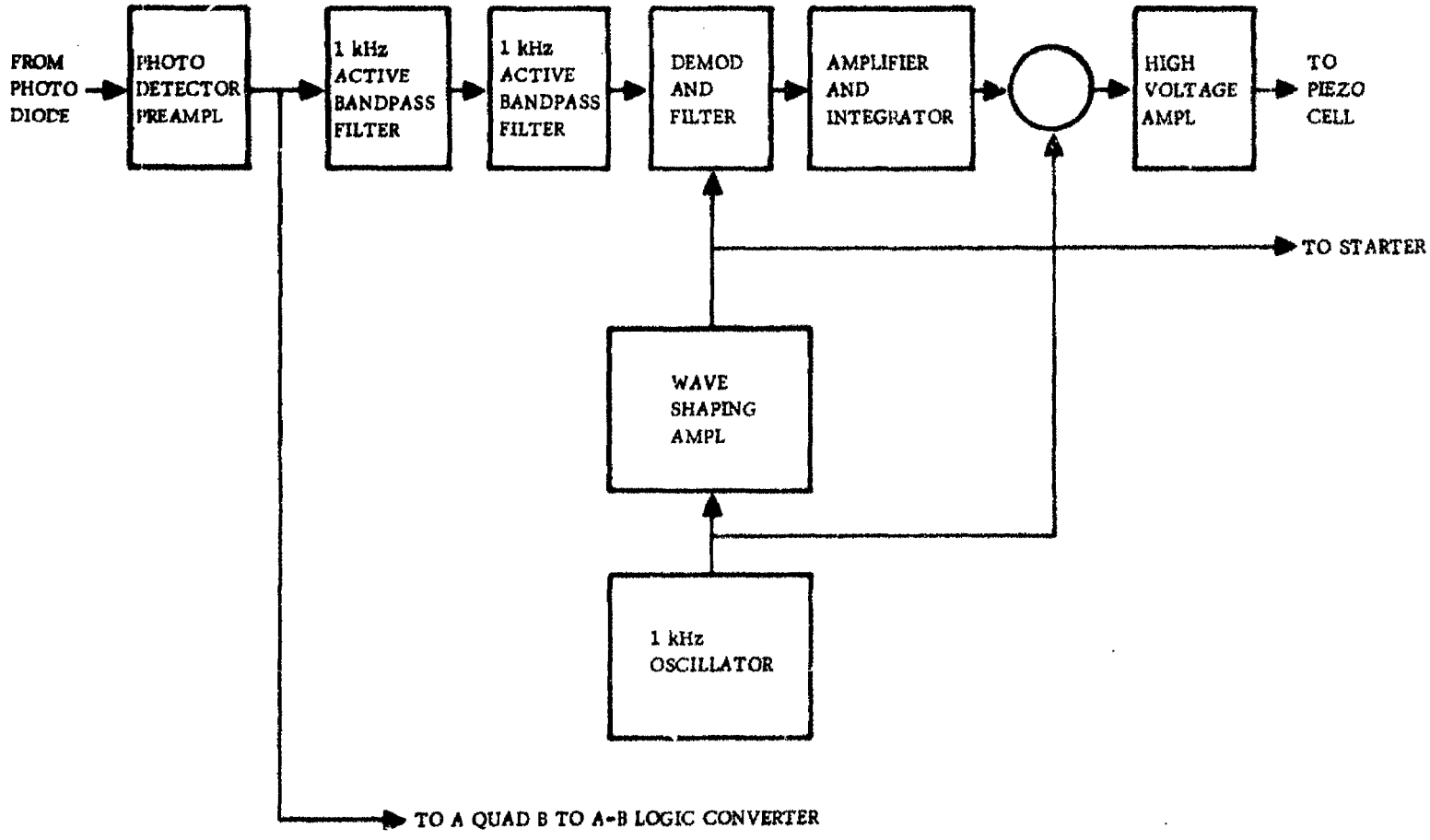

Figure 21. Pathlength Control Block Diagram

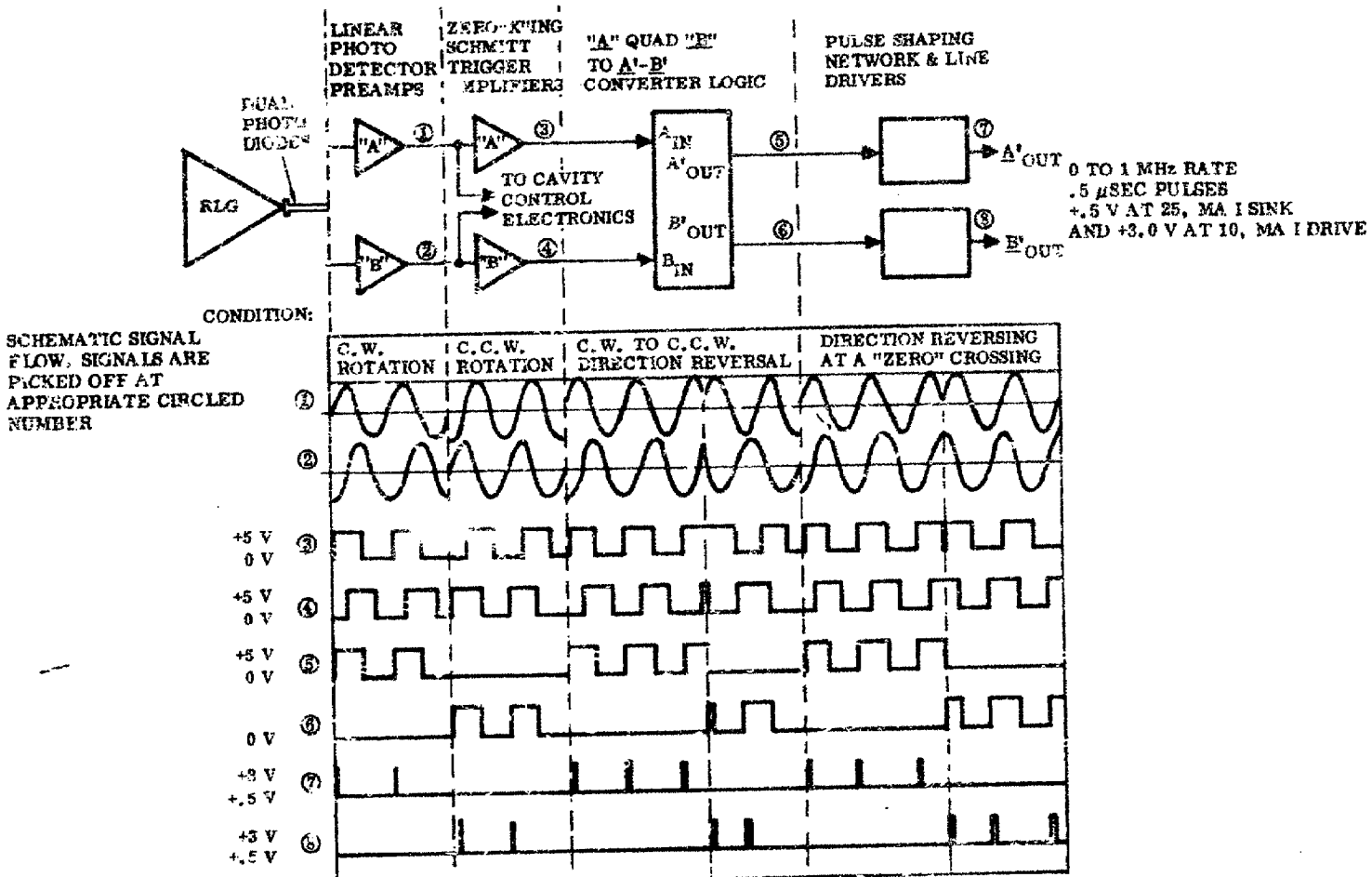

Figure 22. Ring Laser Gyro Readout Signal Flow

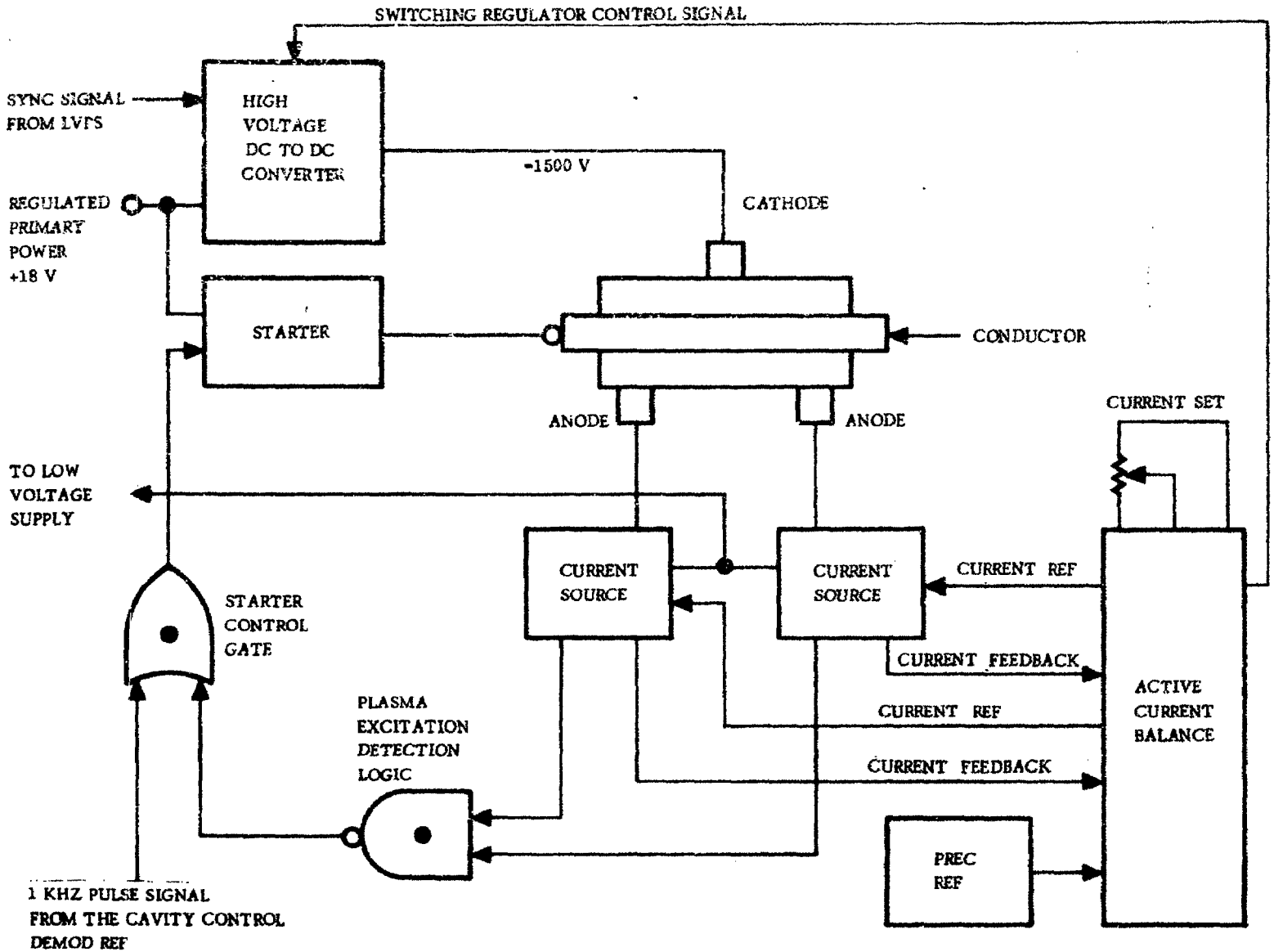

Figure 23. Plasma Excitation Functional Block Diagram

(e) Faraday Bias Electronics. The Faraday bias electronics provide the precision current for the Autonetics anti-lock mechanization. The amplitude and frequencies are maintained very precisely by utilizing ultrastable components in all critical areas. In addition to the careful choice of stable electronic components, the circuits are designed so that positive and negative thermal coefficients are balanced wherever possible.

The scale factors of Faraday bias elements are temperature sensitive. Consequently, the RLG has a separate temperature controller which will maintain its Faraday bias element at a temperature slightly above the laser gyro body. This controller will maintain approximately $\pm 0.05^{\circ}F$ control and has a fast reaction time. This control will fix the optical scale factor of the Faraday bias element.

4. OPERATING PROCEDURE

This section describes the step-by-step operating procedure for readying the Ring Laser Gyro Model RLG-1140 and Electronic Controller Model 717 for functional use. At the completion of this procedure, the instrument may be tested in accordance with any program prescribed by the operator.

Prior to turn-on the RLG should be mounted on a metal base plate which acts as a heat sink for the instrument. The heat sinking capacity of this plate should be equivalent to a convective cooling surface of 200 $in.^2$ area or greater.

The Ring Laser Gyro Model RLG-1140 and Electronic Controller Model 717 are prepared for operation by performing the following startup procedures:

1. Set all controls on the Model 717 Controller in the following positions:

    a. Power switch in OFF position
    b. Gyro Heater switch in OFF position
    c. Pathlength Servo switch in OFF position
    d. Monitor switch in PLASMA CURRENT position

2. Connect P8 to gyro connector J8

3. Connect two lengths of RG58A/U or other 50 to 52 ohm impedance coaxial cable between J12 and J13 and any A-B input format counter with a 1 MHz or higher count rate capability. The coaxial cable must be terminated into a 51 ohm, 1/2 watt ± 10 percent composition resistor at the counter end of the cable. Failure to do so may result in improper counter operation due to coaxial cable ringing. Preset trigger levels of the counter to fire at +1 V and +3 V.

4. Connect P3 and P4 to a well regulated +28 VDC power source capable of supplying at least 2 amp DC continuously. Verify that P3 is connected to the + terminal and P4 to the - terminal. If P3 and P4 are reversed, and applied voltage is less than 50 VDC, then no damage will occur. A protection diode prevents reverse polarity damage.

5. Turn on +28 VDC power source and observe voltage setting. Set voltage to +28 ± 2 VDC. Set current limit control (if present) to a value greater than 2 amp DC.

6. Turn the Power switch to GYRO ON position on RLG Controller. Observe the plasma current on the monitor indicator. It will rise to a value between 8 to 10 ma during startup. After approximately 2 to 3 sec it will fall back to a value of 4 to 6 ma. As soon as the plasma current falls back, then proceed to the next step.

7. Turn on the gyro heater by moving the Gyro Heater switch on the controller to the ON position. Switch the monitor selector to GYRO HTR VOLTS. It should indicate between 0.9 and 1 on a scale of 0 to 1. This reading will be influenced by the setting of the +28 VDC power supply voltage. At +28 VDC, it will read 0.95. Next move the Monitor Selector switch to GYRO TEMP position. Record the reading (refer to conversion tables for gyro temperature value). Next move the monitor selector to BASE PLATE TEMP position and record value (refer to conversion tables for base plate temperature value).

8. After the gyro has been on for several minutes, switch the pathlength controller to ON position. Observe the ±100 μa meter. It may or may not move from 0 initial value depending on where the center of the instrument mode is. However, after some period of time (15 min), it will move off to one side to a reading of 60 to 80 μa. At this point, if the operator so chooses, a mode nearer 0 may be obtained by switching the Pathlength Servo switch momentarily to MODE CHANGE and then back to ON position. The next axial mode nearest 0 will be captured. In no case should operation of the gyro be attempted for sustained periods if the current exceeds ±90 μa. No damage will occur to either the instrument or the controller. However, the dynamic range of the servo will be exceeded, so that there is no assurance that the instrument is operating at the center of the gain curve.

9. After a warmup period of 30 min, the instrument is ready for functional use.

5. RLG-1140 PERFORMANCE TESTS

The experimental performance checkout of RLG-1140 consisted of a setup procedure and a subsequent short testing period. Various adjustments were made after each short test run to enhance the performance of this instrument.

a. Setup Procedure

The mating of the RLG and the control electronics requires many adjustments to be made to prepare the instrument for the tests which establish the performance characteristics. These procedures are summarized briefly below.

The cathode current is first set at approximately the final value as determined by the instruments during the insertion of the Faraday bias element. The Faraday biasing currents are set at nominal values such that the total power drawn by the RLG from the electronic controller unit will be approximated. The unit is next operated until it comes to a thermal equilibrium. The temperature of the RLG is then elevated slightly by the heater controller so that thermal control can be achieved. The apertures are then set to eliminate any off-axis TEM modes from lasing.

At this point all physical adjustments to the laser cavity are completed and the various control loops, e.g., the cavity length servo controller, photodiode detection and counting logic, etc. will now operate. The Faraday bias element temperature controller is then set to maintain the bias element temperature slightly above the temperature of the gyro body.

The final adjustments of the Faraday bias currents for best performance are then completed. After a short period the various control loops are rechecked to make sure that power levels and temperatures are within certain nominal ranges.

The thermal configuration of RLG-1140 was designed for a laboratory environment which would include a mounting flange that would adequately heat sink the RLG. The heaters on the instrument are able to control the temperature of the RLG as long as the temperature of the flange to which it is mounted is maintained within the temperature range of about 65°F to 80°F. The testing of RLG-1140 was conducted with two different heat sinks. One was a 12 in. x 12 in. x 1/2 in. normal convection air-cooled aluminum plate operating in the laboratory ambient at 72°F. The second was a 26-in.-diameter 3/4-in.-thick aluminum plate which represented an essentially infinite sink.

The warmup time from a cold start, i.e., room temperature, is dependent upon the thermal conduction rate from the base of the RLG to the mounting flange and the temperature of the mounting flange. For the two thermal mounting cases given, the times for the thermal controller to come into control range were between 15 and 25 min. The data obtained after a 30-min period generally show good stability.

b. Test Results and Discussion

The performance of the RLG and the electronic controller can be characterized in various ways and each supported with data. Since there is no standard method of displaying the data, several different methods are utilized here to show the performance test results in different perspectives. Comments as to the method and the relative merits of each data set are given below.

The data from several 1-hr drift runs are shown in Figures 24, 25 and 26. Data were taken by accumulating the output pulses of the RLG over a period of 10 sec. In each case the RLG was stationary in the laboratory with vertical earth rate input. These data points then represent the average angular rate over the 10-sec periods. Due to the inherent digital nature of the output of ring laser gyros, the resolution of the data for the interval is one count. Thus each count in a 10-sec interval represents 0.17 deg per hour. Hence, the top line plot of the raw data can be seen to have step function values equal in amount to one or more of these counts. Also due to the inherent nature of the RLG this one count resolution limit is not randomly occurring but is bounded in any given accumulation of the data. That is, the error of one count exists at the end of any accumulation interval and is non-accumulative beyond that. If the input rate to the RLG is constant and any internal biases are constant, then if the counting error is high over one period it must be equally low over the next period. Therefore, the method of looking at the accumulated angles will result in no dependence on time for the data.

The first method of analysis is similar to that utilized by the Naval Weapons Center at China Lake, California, where RLG-1140 was sent for evaluation after delivery to AFAL. The mean and standard deviation from the mean are determined. The standard deviation is then given with the time interval of the measurement. This is called "random drift" and is represented by σ_{10}. The data were then summed into a smaller set by accumulating ten of the original data points. This is equivalent to setting the data recording apparatus to accumulate over a period of 100 sec. The standard deviation from the mean is then given and is shown on the figures as σ_{100}.

The accumulated angular error plots shown on the bottom of each of the data sets are the accumulated angular deviation of the data from the mean. This is equivalent to the instantaneous heading errors due presumably from drifts of the RLG bias with time. Since the raw data can be seen to be trending over the data sets from the start to the finish, all the accumulated angular error plots show the same characteristic trending. If the data were trending linearly with time, these plots would be parabolic in character. Note the vertical scale factor of the figures for future reference.

A second method of analysis is shown in Figure 27. Here all three data sets are plotted on one graph. The bias is determined by measuring the average of the first 10 min of the data set. Then this bias is subtracted from all the remaining set and the residuals are accumulated.

These residuals are then plotted and represent the instantaneous heading errors as determined from the initial calibration period. This is equivalent to a flight where the bias is calibrated initially and the result propagated over the flight. It can be seen that during the period of setup and adjustment of the RLG the heading errors got smaller as various adjustments were made. This is noted by the dates on the data. The data set for Figure 26 was taken for the demonstration of RLG-1140 performance during final acceptance testing. This last test data can be seen to indicate a random drift of less than 0.1 deg/hr.

Another method of looking at these same data would be in light of the possibility that the instrument drifting is due to mechanical strain relaxation and/or possible magnetization relaxation. These and various possible thermal mechanisms could cause long-term trending. If the source could be isolated or a calibration of the apparent bias rate change could be determined, then the performance of the RLG could

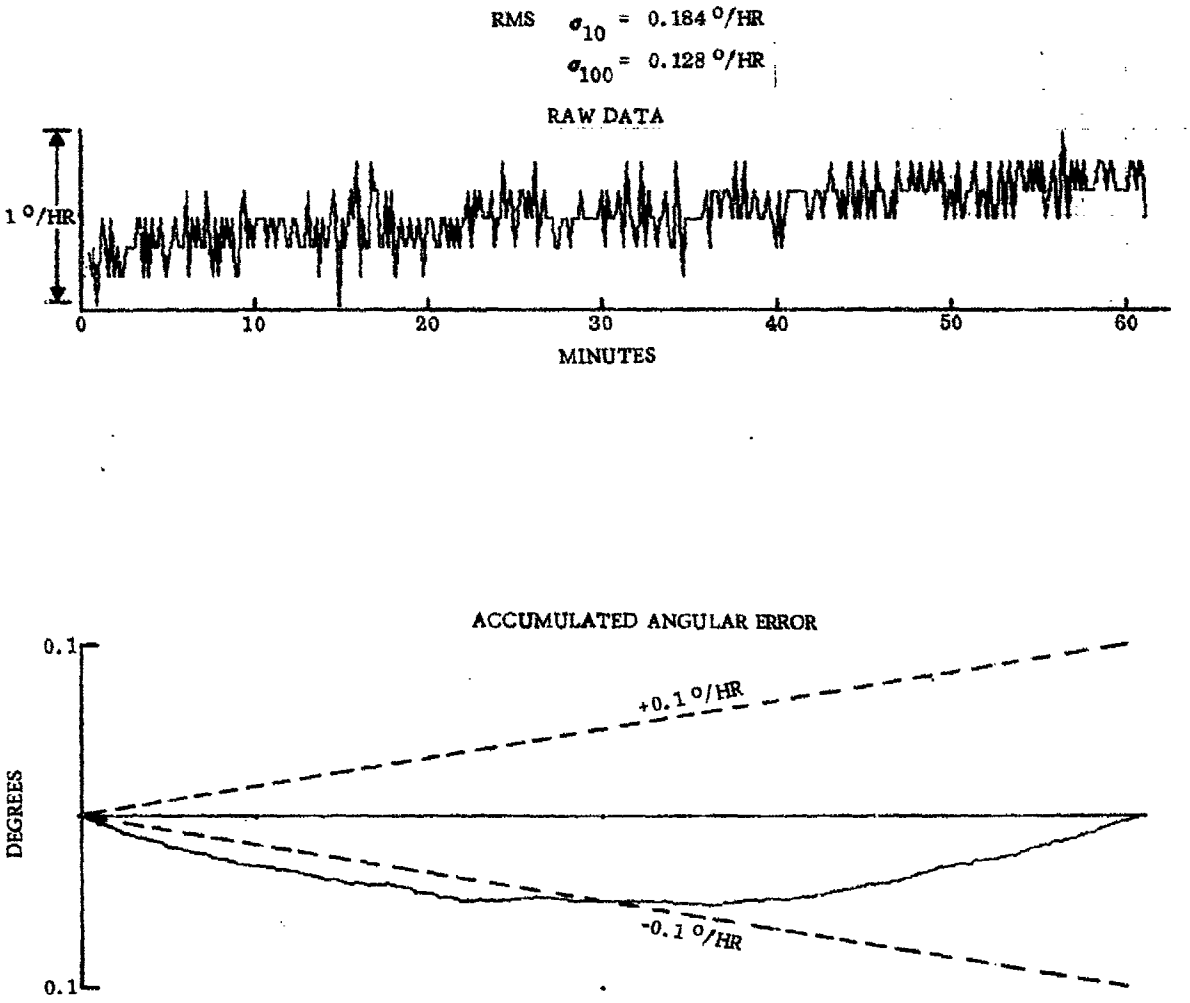

Figure 24. RLG-1140 Drift Run, March 12, 1973

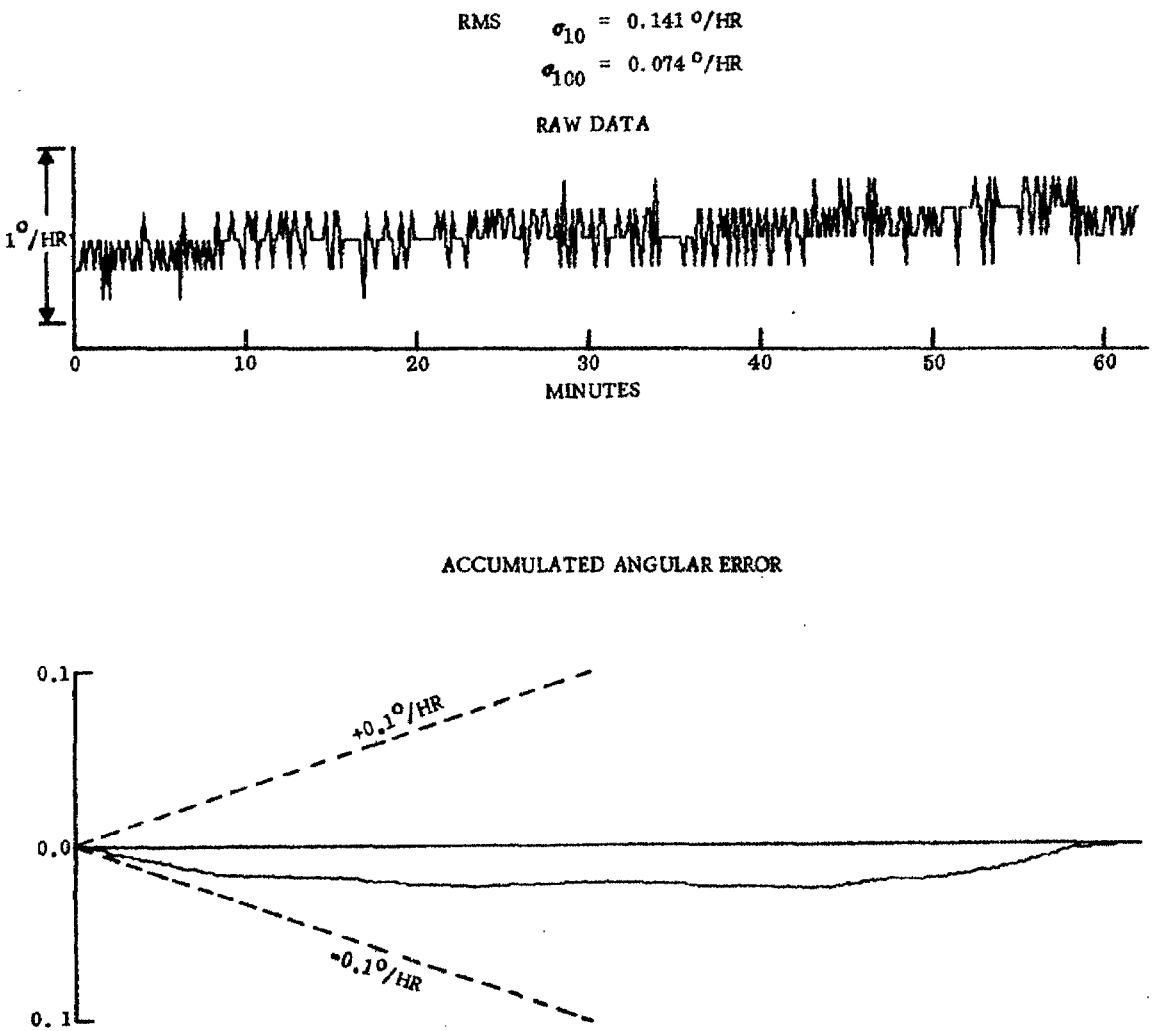

Figure 25. RLG-1140 Drift Run, March 15, 1973

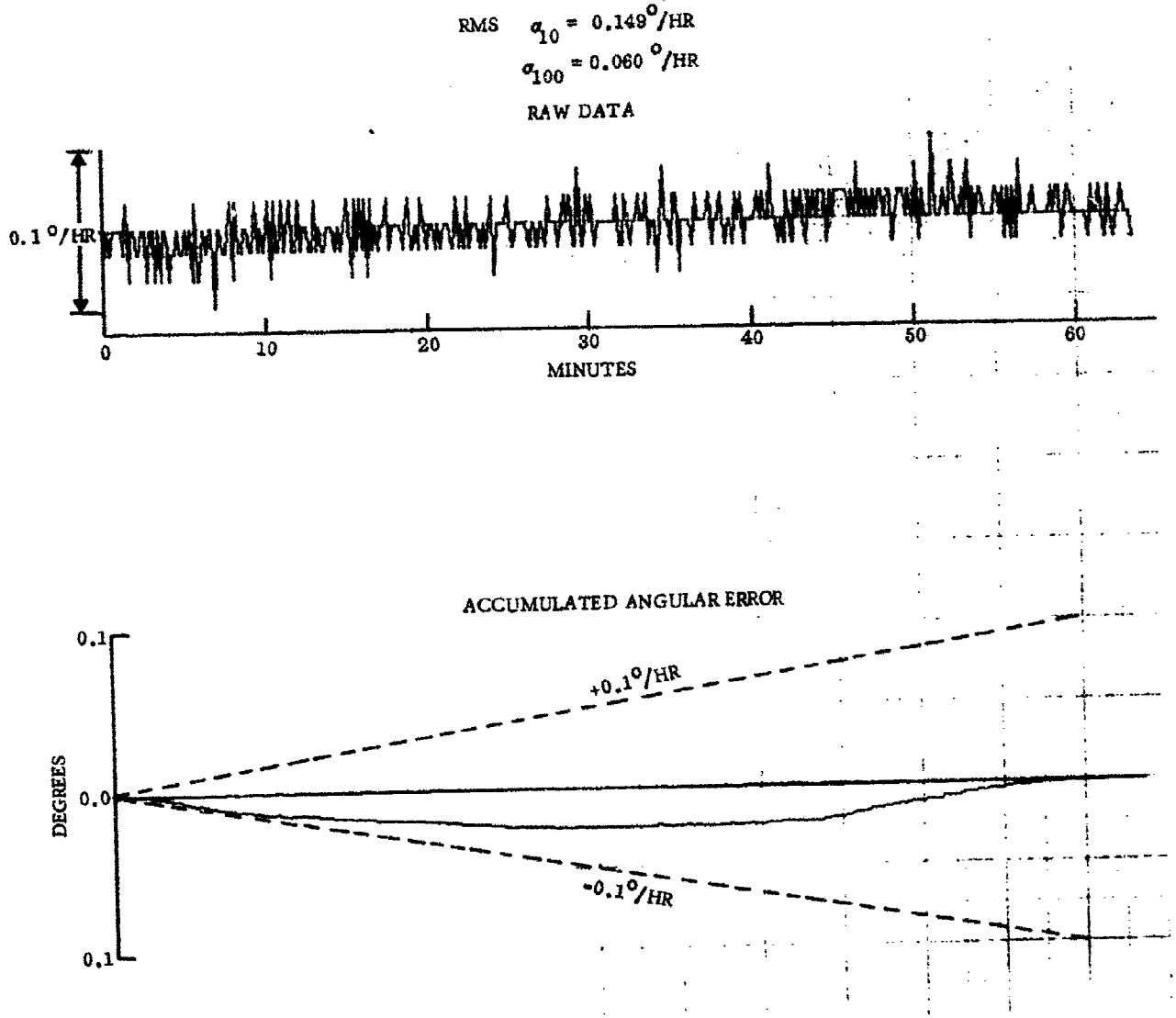

Figure 26. RLG-1140 Drift Run, March 16, 1973

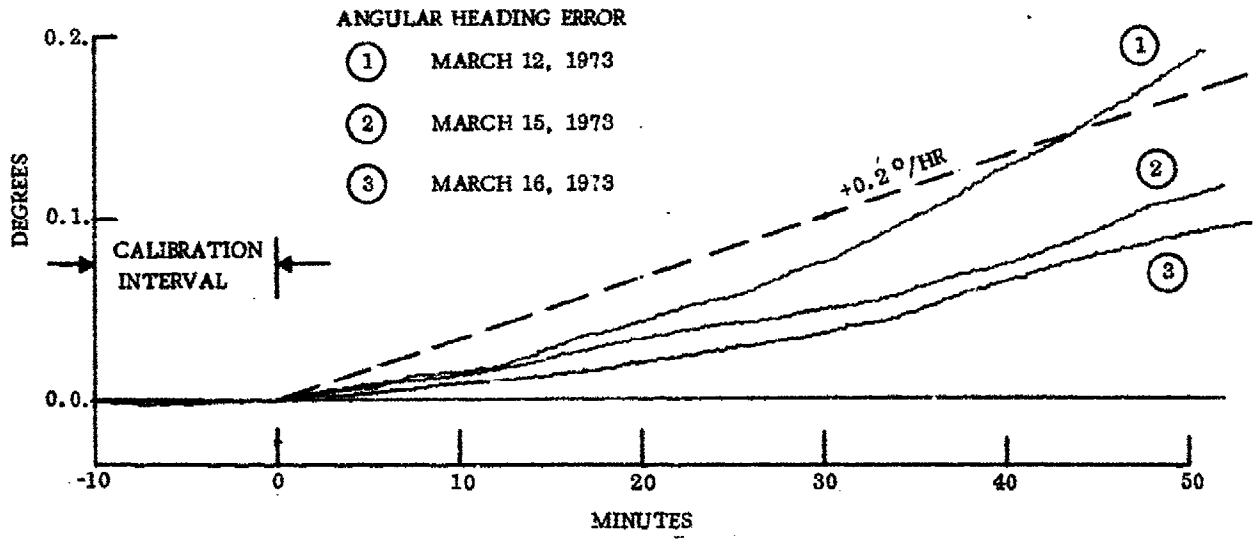

Figure 27. Angular Heading Error

best be shown by fitting the data set with the best-fit straight line. This method is shown in Figures 28, 29 and 30. All plots are similar to those shown previously but note that the vertical scale factor of the accumulated angular error plots is ten times smaller than the previous data plots. The standard deviation from the mean of the residuals accumulated over equivalent 100-sec intervals is shown on the data sets. This method of data analysis shows the potential of the RLG if the sources of the trending are found and eliminated.

One additional drift run was taken. This run had a duration of 60 hr. It is shown in Figure 31. The data were recorded as RLG output pulse accumulations over 300-sec intervals. The rms deviation of the whole set from the mean is shown on Figure 31. The accumulated angular deviation is shown where the calibration interval is the first 30 min of the data run. The warmup period of the unit was about 60 min. Estimates of performance over shorter time intervals can be made by determining the angular variations of the accumulated angle plots over the interval of interest.

The second method of testing the RLG instrument is to determine the scale factor value at various different rates. This is called a linearity test. It is typically done in the following manner. The RLG and controller are mounted on a rate table. The table has a precision angular encoder. The RLG pulses are connected through slip rings to the inputs of an appropriate counter. The counter is then triggered by the angular encoder of the table such that the number of RLG output counts is measured over a known angular interval of the table. When the table is turned at a constant rate the count can then be compared with the time for the table to turn through the angular

σ_{100} = 0.043 °/HR

DATA

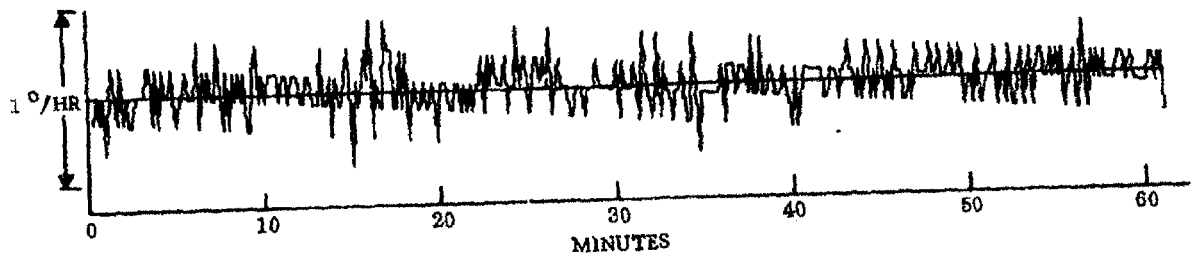

ACCUMULATED ANGULAR ERROR

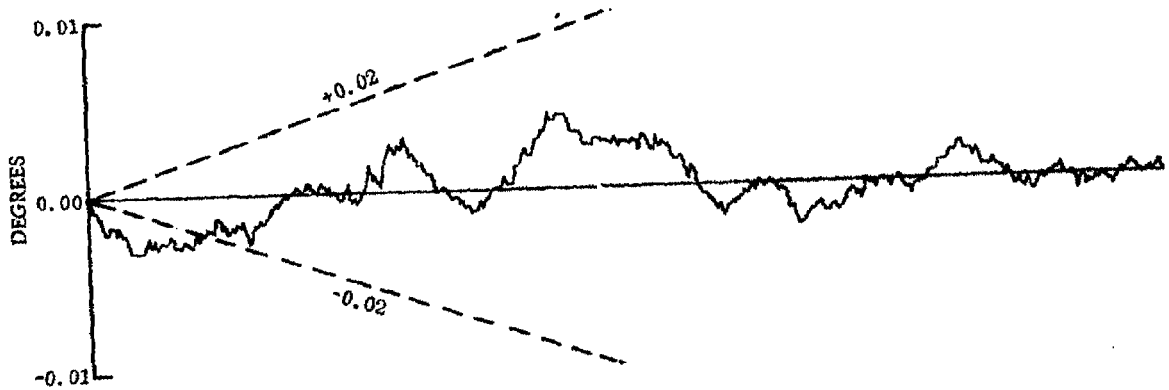

Figure 28. RLG-1140 Drift Run, March 12, 1973 (Slope Removed)

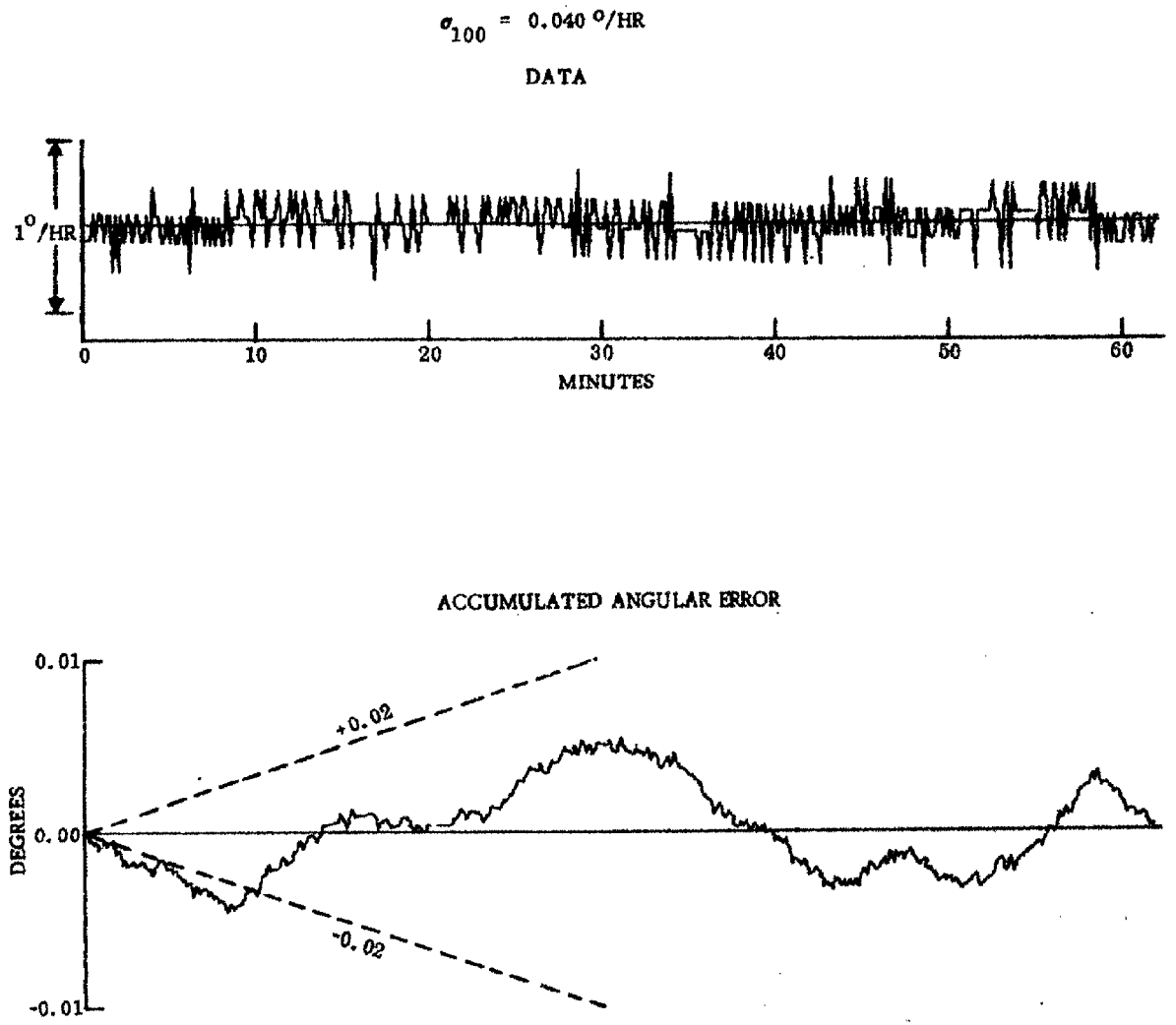

Figure 29. RLG-1140 Drift Run, March 15, 1973 (Slope Removed)

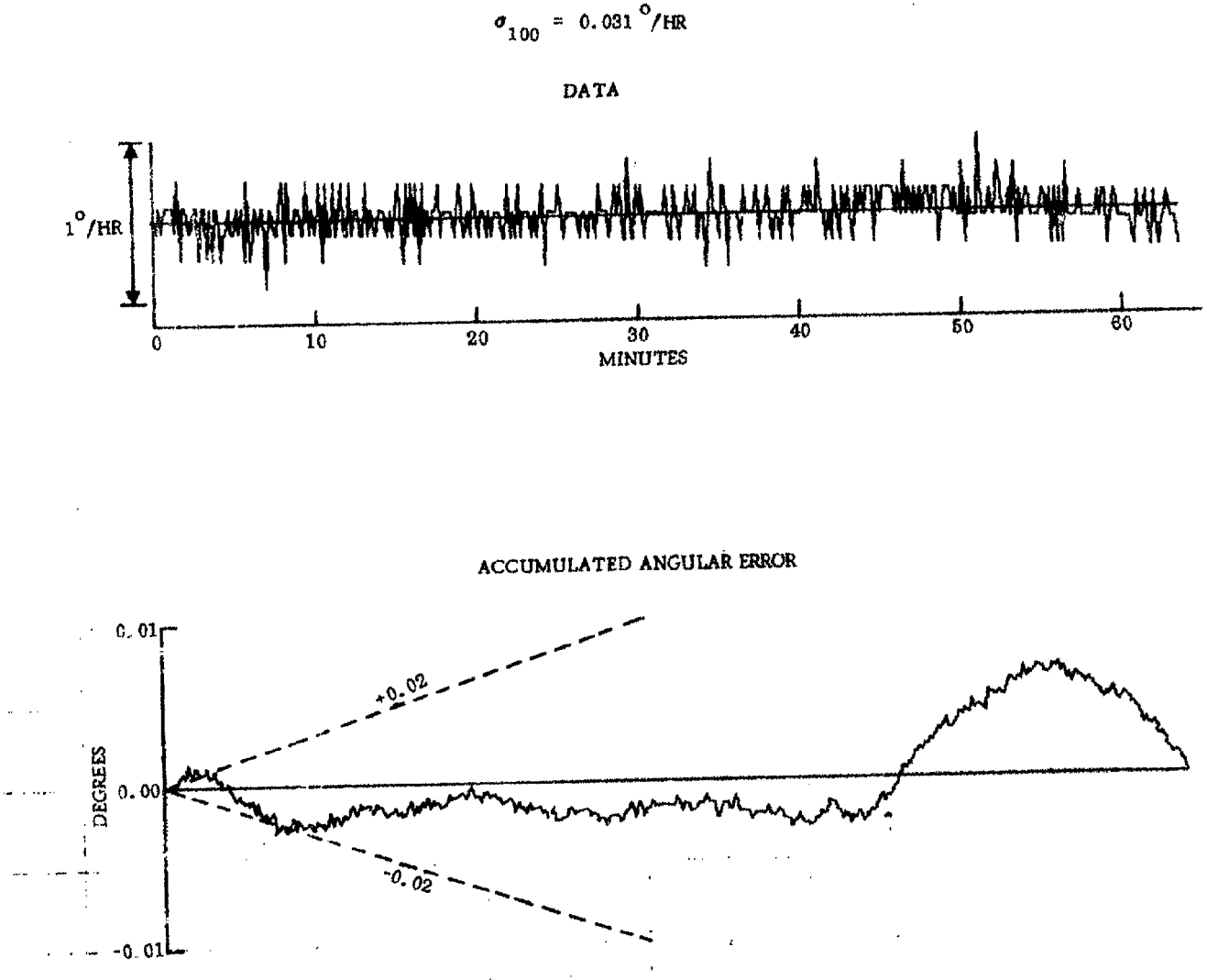

Figure 30. RLG-1140 Drift Run, March 16, 1973 (Slope Removed)

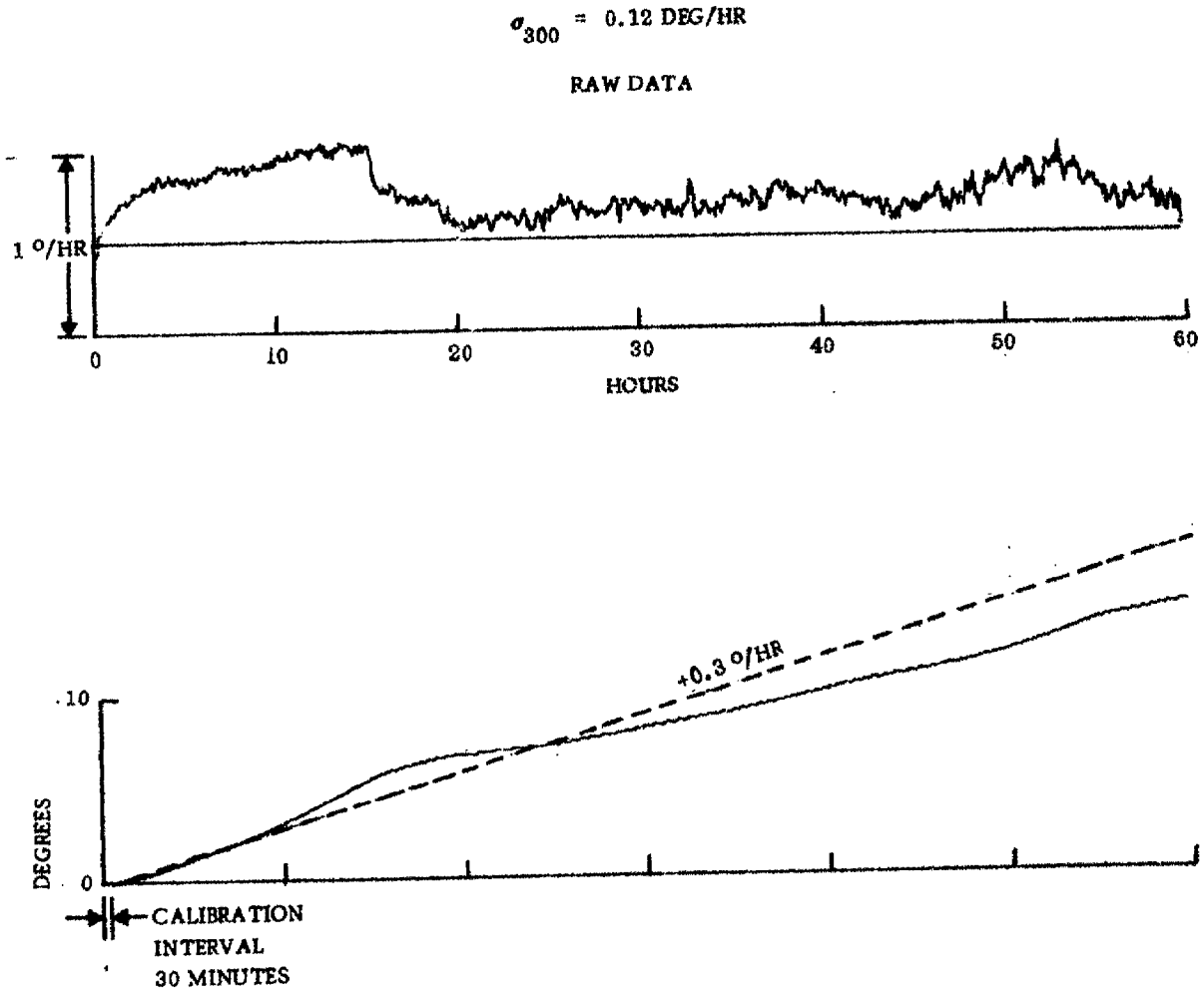

Figure 31. RLG-1140 Drift Run, March 16 to 19, 1973 (σ_{300} = 0.12 deg/hr)

interval, and the equivalent scale factor can be determined. The bias present in the RLG must be measured so that any pulses present due to instrument bias can be subtracted from the count. In addition, the earth's rotation must be added or subtracted as the case may be. The resulting data from this type of test are shown in Figure 32. The table rotation rates were 0.1, 1, 10, 50, and 100 deg/sec. At the lower rates the determination of the exact value of the bias present becomes very important since a slight variation of the value will lead to a rather large error in the scale factor determination. This is demonstrated by the two data points shown at 0.1 deg/sec. These points are the same data with the analysis using first the bias measured before the linearity run and then using the bias measured after the data run. It can be seen that the two variations cause a symmetric splitting which reverses from one bias value to the other. This indicates that the bias during this measurement was somewhere between the two values before and after the runs. The zero-to-peak excursion of the data set is about 0.05 percent.

In summary, the data presented show that the RLG-1140 instrument has the potential for very good performance. The main detracting characteristic is the long term trending that is present on most of the data. This trending may be reducing with time; however, the interval over which the instrument was observed was too short to determine this positively. The source of the trending may be magnetic or mechanical in nature and hence would be of thermal origin since both of these effects are temperature sensitive. The performance of RLG-1140 when placed in a stable thermal environment with a temperature-controlled mounting plate would be expected to be very good, i.e., 0.02 deg/hr.

6. RING LASER GYRO RELIABILITY

a. Reliability Prediction

A preliminary reliability prediction for an RLG system containing one instrument plus electronics was performed in accordance with MIL-STD-756A using the part class and part type method described in Para 4.5 of MIL-HDBK-217A. The preliminary reliability prediction, which is summarized in Table II, gives an MTBF of 3270 hr for an aircraft environment using the airborne use environment factor from MIL-STD-756A. Specific conditions regarding environmental and electrical stress on parts, component parts reliability grades, parts failure rates, and design maturity embodied in the prediction are as follows:

(1) Temperature

The prediction is based upon a baseplate temperature of 160°F. Temperature rises above the baseplate temperature to component cases and semiconductor junctions were estimated from a preliminary thermal model.

(2) Parts Reliability Grades

All discrete passive components will be MIL-ER reliability grades. All discrete semiconductor devices will be JAN-TX grades per MIL-S-19500. All integrated circuit semiconductors will be Class B devices per MIL-M-38510. All parts in the categories described above which are not available under military procurement specifications will be procured to Autonetics IID specifications which contain either identical or equivalent screen test requirements to assure the intended reliability grade.

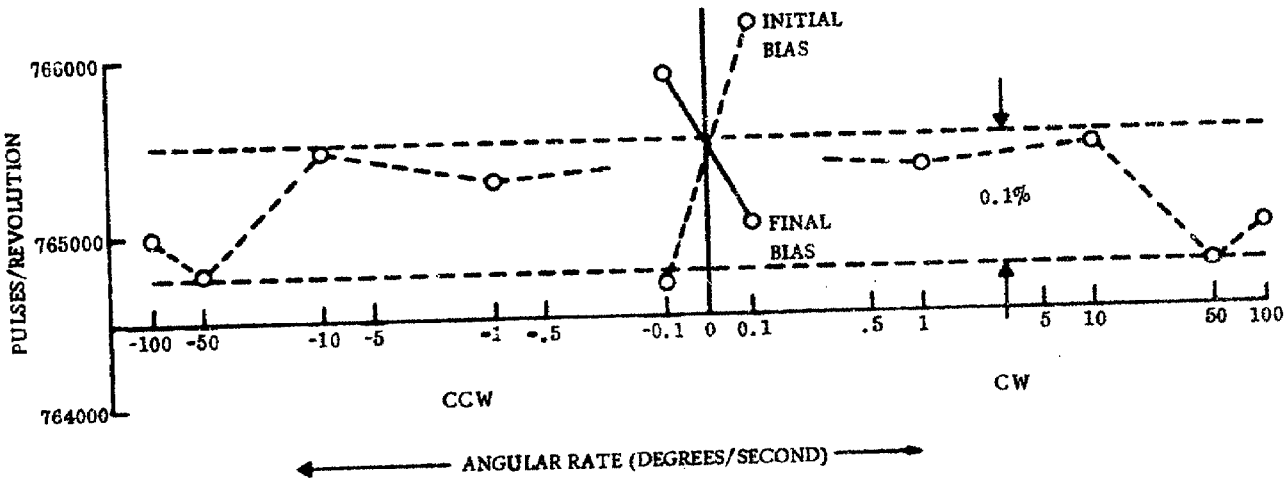

Figure 32. RLG-1140 Linearity

Table II. Ring Laser Gyro System Reliability Prediction Summary

Item	Failure Rate (%/1000 Hr)
40-cm RLG	2.167
Photodiode Buffer Ampl	0.169
Electronics	
Cavity Length Control	1.081
Faraday Driver	3.977
Gyro Temperature Controllers	1.032
Signal Generator	1.641
Current Sink	2.746
Power Supplies	
Low Voltage Power Supply	16.250
High Voltage Power Supply	0.989
MIB and Connectors	0.533
Total Failure Rate = 30.585 %/1000 hr	
MTBF = 3270 hr	

(3) Hybrid Microcircuits

All hybrid thick- or thin-film microcircuit assemblies will be screened to comply with MIL-STD-883, Method 5004, Class B screening procedures and requirements.

(4) Design Maturity

The predicted MTBF is the nature design reliability of the ring laser gyro system in the application environment.

(5) Part Failure Rates

The failure rates used for the various electronic components were obtained from sets of component failure rate curves for the appropriate reliability grades maintained by Autonetics. These failure rates correspond well with outside sources such as MIL-HDBK-217A and the RADC Reliability Notebook, Volume II, and check well with component achieved failure rates from Autonetics programs including F-111 and Minuteman II and III.

(6) Hybrid Microcircuit Failure Rates

Failure rates for hybrid microelectronic assemblies are obtained using a preliminary prediction technique which considers contributions to assembly failure rate for the circuit substrate, screened resistors, active and passive chip components, and electrical interconnecting bonds including flying wire ball and wedge bonds. The failure rates used for chip resistors and capacitors are the same failure rates used for comparable cased parts of the equivalent reliability grade in the Autonetics failure rate data set.

(7) Component Electrical Stresses

Electronic component failure rates were calculated for the principal reliability determining electrical stress parameters applicable to a given part type using average or typical stress ratios characteristic of Autonetics electronic circuit designs.

(8) Ring Laser Gyro Failure Rates

Failure rates used in the prediction for the ring laser gyro instrument itself are the nominal values obtained using the estimating methods described in subsequent paragraphs of this section.

b. Future Reliability Improvement

The long-term objective for Autonetics hybrid microelectronics designs is the full use of Beam-Lead, Sealed-Junction (BLSJ) semiconductor devices. BLSJ devices, developed by Bell Telephone Labs and first used on the Safeguard Program, were specifically developed to eliminate the predominant failure modes of conventional oxide-passivated semiconductor devices with aluminum metallization systems. Test data show that the basic failure rates of BLSJ devices are lower by factors of two to ten over comparable conventional devices. The reduction in failure rate of a ring laser gyro system with a full complement of BLSJ semiconductor devices (except power supplies) was examined. The predicted MTBF with BLSJ devices is 3620 hr.

c. Ring Laser Gyro Reliability

The ring laser gyro is a new instrument with respect to service in military weapon system equipments. Accordingly, there are insufficient use and experience data available on ring laser gyros or similar instruments to support a quantitative reliability forecast. The approach taken to formulate a reliability estimate for ring laser gyros involves examining the design and construction of the instrument and an analysis of its failure modes in terms of the intended application.

(1) Design and Construction

The ring laser gyro is an instrument of extreme inherent simplicity in terms of the number of separate parts involved in its construction. It is not without critical dimensions and parameters on which performance will depend, but the fact that so few separate parts are involved limits the number of failure modes and mechanisms in the instrument. The technology to fabricate parts and the assembly processes required are available and, in some cases, are routine.

(2) Failure Mode Analysis

A preliminary failure mode analysis of the ring laser gyro instrument is contained in Table III. Part A of Table III is an examination of dormant and storage failure modes. Part B of the table describes the operating failure modes. In performing the preliminary failure mode analysis (and in constructing Table III), it was the intent to identify all reasonable and practical failure modes, both dormant and operating, and to identify their sources and causes. The very fact that a certain potential failure mode is included in the table, e.g., mirror degradation or structural failures, does not imply that failures from the causes and mechanisms listed will ever occur. The purpose of including all possible failure modes is to identify all the factors which need to be considered in the design of a reliable instrument. In this respect, certain design actions, analyses, and tests which should be accomplished can be identified from the table.

The failure modes which are believed to be significant are loss of helium gas atoms and contamination for dormant failures and pumping gas loss and mirror degradation for operating failures. The storage failure modes also could be operating failure modes, but operating time and operating life are sufficiently short with respect to storage time to make these failure modes insignificant as operating considerations in well designed instruments.

(3) Preliminary Reliability Estimate

The inherent simplicity and the small number of failure mechanisms in the ring laser gyro instrument, together with the fact that the opportunity can exist to direct advanced development efforts to meet specific environmental and reliability requirements for aircraft application, implies that a ring laser gyro system will be in a reliability class of instruments with MTBF's much greater than current electromechanical designs. While ring laser gyro reliability cannot be estimated from electromechanical instrument achieved data, the ring laser gyro can be compared regarding its general reliability class on the basis of number of failure modes and inherent complexity. Existing electromechanical instruments, including single-axis floated rate integrating gyroscopes and pendulous velocity meters have achieved MTBF's ranging from 5,000 to 100,000 hr (ground environment). In many cases, these achieved MTBF's include wearout failures in addition to "chance" or random failures within instrument useful life. Considering the complex fluid systems, rotating elements, seals; and the rolling and sliding contacts, etc, present in these instruments, as well as the relatively large numbers of parts per assembly, an order of magnitude improvement in reliability for the ring laser gyro class is reasonable. Further, considering the reliability projected for recent state-of-the-art instrument designs, improvement by a factor of 20 is possible.

Considering a reasonable improvement factor of 10 projects the preliminary ring laser gyro MTBF estimate within the bounds shown in Table IV.

Table III. Ring Laser Gyro Failure Mode Analysis

Part A. Storage Failure Modes

Failure Mode	Cause/Mechanism	Remarks
Loss of He/Ne Gas	Loss of He/Ne gas through ULE titanium silicate body, fill tube and seal, and the several cement joints and seals at the three mirror assemblies, the two windows, the getter feedthroughs, and the anode and cathode terminals.	The loss rate can be calculated for the ULE body, but must be determined experimentally for epoxy seals and joints. The possibility of using alternate materials or of applying exterior coatings of low permeability materials can be investigated.
Contamination	Contamination of the laser gas and mirror surfaces may arise from two sources: (1) outgassing of internal metal parts (cathode assembly, anodes, and getters) and the laser body. (2) penetration of water vapor through the several epoxy cement joints.	Specific development activities and tests have been undertaken to reduce the failure rate to an acceptable level for a one-year storage time. These activities involve the design, choice of materials, fabrication and assembly processes, stabilization bake, evacuation and fill methods, etc. Exposure of the RLG to humidity will be minimized by package and storage container design.
Mirror Degradation	Long-term deterioration of mirror optical and filtering qualities due to plating cracking or separation, change in optical properties, or absorption of contaminants.	This failure mode will be insignificant provided that good plating process control is maintained. The processes required are otherwise fairly routine. Multiple-layer platings are involved.
Dimensional Stability (Long Term)	Age-related relief of internal, machining, and forming stresses in materials and bonds.	This failure mode can be evaluated only by storage life tests.

Table III. (Cont)

Part B. Operating Failure Modes

Failure Mode	Cause/Mechanism	Remarks
Mirror Degradation	Degradation of mirror optical quality and efficiency as a function of operating time caused by ion bombardment.	Severity of this failure mode is related to the contamination level (see Part A).
Accelerated (Pumping) Gas Loss	Gas loss occurs when gas atoms, ionized by the strong electric field, are accelerated into the cathode material by electrostatic forces. Collision with the cathode may result in burial of the ion.	The mechanics of pumping depend highly on certain parameters of the design which may be influenced to minimize the loss of lasing gas ions. Examples of these parameters are cathode material, surface preparation, current density, and geometry.
Piezoelectric Device Failure	Failure of the piezoelectric mirror drive stack due to change in properties, plating separation, or solder and epoxy bond failures.	No failures of piezoelectric devices have been experienced after device fabrication in laser development tests.
Electrical Failure	Failure of either of two photodiodes or the electrical connections to the diodes, anodes (2), cathode, piezoelectric stack, or Faraday package.	A predicted failure rate for the RLG electrical failures noted here is 0.01 %/ 1000 hr
Dimensional Stability Under Environment	Intermittent failure of the RLG due to distortion of structures or components under the forces of mission environment.	Structural distortion beyond acceptable limits and structural failure should not be expected in production RLG's designed (and proved by Qualification tests) to operate in the mission environment, except when workmanship and material defects may escape inspection and reliability screen tests.
Structural Failure Under Environment	Catastrophic failure of the RLG due to breakage, slippage, or separation of components under the forces of mission environment. This includes failures of components within as well as outside the plasma section. Breakage of parts within the plasma section will cause the lasing mixture to be contaminated (gain reduction). Movement of parts outside the plasma, such as separation of the Faraday parts or displacement of the aperture, may cause increased losses and result in the ceasing of laser action.	

Table IV. Projected Ring Laser Gyro MTBF Range
(All MTBF's Specified for Fixed Ground Environment)

Conventional Electromechanical Instrument Achieved MTBF (hr)	Minimum	Nominal	Maximum
	5,000	30,000	100,000
Using a reliability improvement factor of 10			
Ring Laser Gyro Projected MTBF (hr)	Lower Bound	Nominal	Upper Bound
	50,000	300,000	1,000,000

Selecting the nominal value above and relating it to an airborne environment gives 46,000 hr MTBF for the RLG in the reliability prediction.

7. RING LASER GYRO MAINTAINABILITY

Maintainability is defined to be the probability that an item will be retained in or restored to a specified condition within a given period of time, when maintenance is performed in accordance with prescribed procedures and resources.

For a ring laser gyro system, as for any other system, there are two forms of maintenance – corrective and preventive. Either one or a combination of these may be used to maintain the ring laser gyro within its performance specification.

a. Corrective Maintenance

Corrective maintenance is the action performed, as a result of a failure, to restore an item to specified conditions (Ref MIL-STD-721B). The maintenance action to repair a ring laser gyro system after it has failed is made up of several individual tasks, and the sequence of performance of these tasks is referred to as the corrective maintenance cycle. The cycle is divided into four functions: (1) detection of the trouble, (2) determination of the action necessary to correct it, (3) replacement of the faulty item, and (4) adjustment and checkout of the equipment and its return to service. The four functions are, in turn, divided into individual time elements according to the maintenance tasks.

Any failure in the ring laser gyro system which would cause it to malfunction would be identified and corrected by following the above procedure. For example, if gyro output pulses failed to appear on the output lines, several sources may be at fault. One is that the instrument may not be lasing. If the instrument is not lasing, its gain may have dropped due to deterioration of the plasma section. This would be true if the getter deposits were used up or if the plasma discharge color had degraded. In this case it would be most expedient to replace the plasma section. Lasing may also have stopped due to an increase in cavity loss. The bias package and apertures would then require checkout and replacement if necessary. Electronic problems may also have occurred. For example, due to a power supply malfunction, the tube may not lase because it is not discharged. Another source may be a failure in the logic which is used to process the output pulses.

In any of the above situations, as well as others which may be responsible for system malfunction, the problem must first be identified before the remedy can be implemented and the equipment checked out.

b. Preventive Maintenance

Preventive maintenance is the action performed in an attempt to retain an item in a specified condition by providing systematic inspection, detection, and prevention of incipient failure (Ref MIL-STD-721B).

The preventive maintenance action may consist of any one or all of the tasks identified in a corrective maintenance cycle. The method for controlling and scheduling preventive maintenance is usually predicated upon two factors: (1) the number of hours the equipment has been operating, or (2) the degradation of the performance of the equipment.

Preventive maintenance based upon the measurement of performance to determine whether the equipment is operating within the allowable design parameters may be a more realistic procedure than attempting to control preventive maintenance by equipment operating time. At least this procedure should be considered until some operating history is acquired that could be used to schedule preventive maintenance more effectively. As an example, it may be decided to replace the ring laser gyro instrument when its output intensity has dropped a specified percentage from its initial value.

Providing adequate and accessible test points in the equipment would facilitate preventive maintenance as well as corrective maintenance. However, test points should be carefully designed, so that they do not interfere with the functional capability of the circuits.

The packaging of components and subassemblies in self-contained functional units facilitates the maintenance of equipment and should be the first consideration in designing for maintainability. Properly employed, functional modularization greatly simplifies troubleshooting by making possible the rapid location of faults. Once a fault has been located to a module, it can be quickly removed and replaced by a functionally sound, interchangeable module. Functional modularization makes possible major reductions in the requirements for maintenance technicians and training. Overall requirements for maintenance manuals and technical information are also reduced.

c. Human Factors Aspects of Maintainability

Because maintainability is concerned to a great extent with the maintenance of systems and equipment by people, there is a close and overlapping relationship between maintainability and human factors. In dealing with the subject of maintainability, it must be kept in mind that the design of the equipment has a direct effect upon the individuals who have the responsibility for maintaining the equipment in an operational state. The establishment of a maintainability concept or design is not complete without considering the human factors in the system. This interface can best be accomplished by coordinating the maintainability effort with those who are specialists in human factors engineering, just as it is important to coordinate with other engineering disciplines such as safety engineering, reliability, etc.

d. Availability

> "Availability is a measure of the degree to which an item is in the operable and committable state at the start of the mission, when the mission is called for at an unknown (random) point in time" (Ref MIL-STD-721B).

The availability of a ring laser gyro system is an important quantity to be specified. It is directly affected by the maintainability and the reliability of the system. The following mathematical expression illustrates the point.

$$A = \frac{MTBF}{MTBF + MTTR}$$

where

A = Availability

MTBF = Mean Time Between Failures

MTTR = Mean Time to Repair

Examination of the equation for availability reveals that tradeoffs between reliability and maintainability are possible in order to achieve the desired availability. As an example of the use of this expression, the required MTTR may be calculated if the MTBF and the required A are known. If it is assumed that A = 0.95 and MTBF = 3620 hr (from Section 6), then an MTTR of 190 hr is determined.

In order to effect an improvement in availability over this value of 0.95, it is necessary to determine the exact tasks and the costs to perform the tasks required to obtain the desired availability through either an increase in MTBF or a decrease in MTTR. These costs then provide the basis for further refinements to the MTBF and MTTR. Theoretically, the ultimate goal is to adjust the MTBF and MTTR until the costs to provide the desired availability goal are minimized. In all cases the total costs of solving the problem must be included. These costs include not only the changes to the hardware and installations, but must include costs for changing maintenance manuals, changing the supply and support requirements, retraining of maintenance personnel, etc. The costs must also be calculated over the useful life of the equipment to determine the optimum cost effectiveness solution to the problem.

e. Reliability Failure Rate Curve

To bring the relationship of reliability to maintainability into even sharper focus, the standard reliability failure rate "bathtub" curve in Figure 33 is presented. The "bathtub" curve, as illustrated, is characterized by the three most common types of equipment failures.

First, there is an initial time of high failures called "infant mortality," which is associated with the normal design, manufacturing, and quality control problems generally encountered in the initial phase. (Reference area T_{IM}.) Second, a period of time exists, after the initial problems have been resolved, which is termed the normal operating period of relatively low random failure rates. (Reference area T_{NOP}.) In the third period, failures begin to rapidly increase due to parts "wearout." (Reference area T_W).

The vertical line identified as "Estimated Life" is considered to be the point in time reached wherein the cost of repairing and replacing wornout components plus the inconvenience and costs of increased "downtime" for repairs makes it unprofitable to maintain the equipment in service.

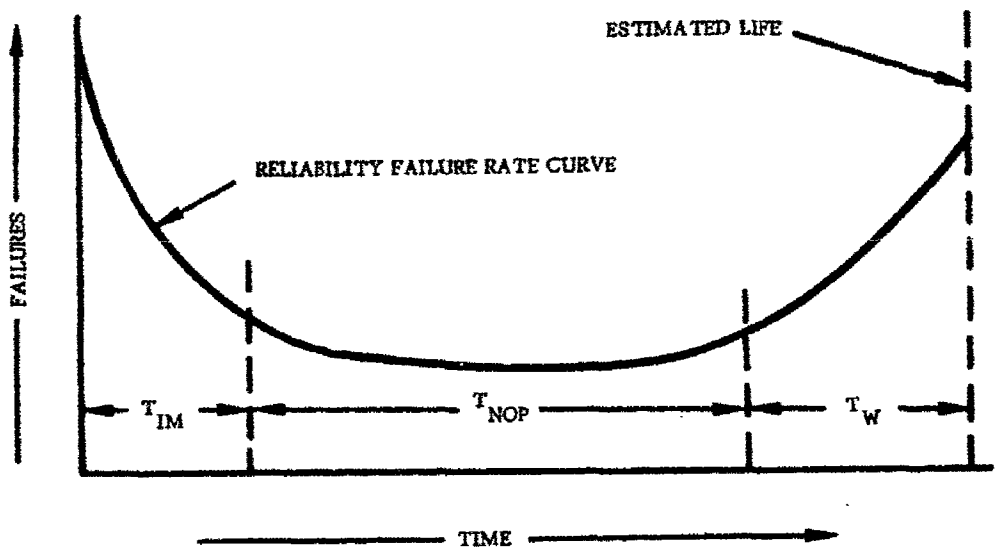

Figure 33. Reliability Failure Rate Curve

Some doubt exists as to whether the standard failure rate curve shown applies to ring laser gyro systems. The RLG system failure rate curve is a composite of the curves for the instrument and electronics separately. The ring laser gyro electronics probably do follow a standard failure rate curve, but the instrument may not. Several known failure mechanisms for the instrument do not obey the normal failure rate curve. Examples of such mechanisms are contaminant gas evolution and helium loss through permeation. Both of these will produce a low failure rate initially and then a much higher failure rate later. Both when permeation loss has produced a significant pressure drop and when contaminant gas evolution has used up all the getter deposit, failures will increase drastically. Because of these effects and others, the instrument failure rate curve should be investigated more thoroughly.

f. Repair/Discard

In the determination of an optimum maintainability policy, the question constantly arises as to whether or not it is more practical or economical to design subassemblies or modules for repair or discard. From a maintainability viewpoint, the optimum design would provide for rapid and unambiguous fault isolation to a low cost nonrepairable throwaway plug-in module. The discard alternative reduces the need for skilled technicians at various levels of maintenance, facilities for repair, detailed and complicated maintenance manuals and procedures, spare parts inventory, identification and control, costly tools and test equipments, scheduling and maintenance hours control, as well as the need for sophisticated and exacting administration. Also eliminated is the need for expensive protective packaging and the handling and transportation of failed modules to the repair site. From this observation, it would appear that designing for discard would be the ultimate goal.

However, this will probably not be possible for a ring laser gyro system. The ring laser gyro electronics can be designed and built mainly in modular form to facilitate maintainability. Whether an electronic module is repaired or discarded when it fails depends to a large extent on whether it is economically feasible to make discardable modules in the quantity required. If this is not economical, then a smaller number of extra modules may be built. Then a faulty module may be replaced with a new module while the faulty one is repaired to act as a backup.

The ring laser gyro instrument will likely require repair or discard as a unit. The instrument itself is not readily adaptable to buildup from individual modules. Also, replacement of elements in the optical path requires recalibration. Again, as with electronic modules, there is the question of repair or discard. Because the instrument is more complex and expensive than most electronic modules, a discard policy would require production in a larger quantity. If this is not the case, then a malfunctioning instrument would be replaced as a unit. The malfunction would be repaired, so that the original unit could be used as a backup instrument.

g. Test and Evaluation

Up to this point, most of the maintainability effort described would be conducted in a theoretical manner. Just as prototype or preproduction hardware is produced to prove the functional theory of the design, so should a means be employed to verify the maintainability aspect of the design. A part of the benefit from the maintainability prediction process is the identification of problem areas that allows for corrective action. This would indicate that the identification of and the solutions to maintainability problems via the prediction process is positive. However, the availability and the validity of the data used in the prediction process may be suspect, particularly in reference to advanced state-of-the-art equipment such as a ring laser gyro system. This then would indicate a need to perform some kind of maintainability testing and evaluation to assure that the equipment does, in effect, conform to the maintainability requirements of the system.

This testing process may deal with only certain suspected elements of equipment maintainability or it may, in the case wherein the prediction process indicates no maintainability problems, be a random selection of tests to prove the adequacy of the predictions. Some method for testing and evaluating the maintainability of the equipment prior to formally demonstrating to the customer that the equipment will satisfy the contracted requirements is needed. It should also be noted that the further downstream in the design, development, and acquisition process the maintainability tests and evaluation take place, the greater is the probability that problems uncovered by this process will be not only costly to solve but will have an adverse effect upon schedules.

For a ring laser gyro system, effort should be concentrated on determining the reliability failure rate curve for the instrument proposed. If possible, early in the program several earlier instruments of similar design should be put on life test to determine precise failure mechanisms.

8. RING LASER GYRO SYSTEM SAFETY

System safety is defined in MIL-STD-882, 15 July 1969, as "The optimum degree of safety within the constraints of operational effectiveness, time and cost, attained through specific application of system management and engineering principles throughout all phases of a system's life cycle."

The general objectives of a ring laser gyro system safety program are as follows:

1. Identify all the hazards related to the ring laser gyro as early as possible.
2. Specify design requirements to eliminate or minimize the hazards identified.
3. Validate that corrective action has been taken in the form of design, safety devices, procedures or warning notes, and signs.
4. Feedback test and operational use information to be considered in future designs and/or modifications to the ring laser gyro system.
5. Establish and maintain accurate records which can be used to defend product liability suits.

At this time most of the safety hazards related to the ring laser gyro can be identified. These main areas of concern are the lasing output, the high voltage required for discharging the plasma tube, and implosion. The hazardous effects of high voltage and implosion are well-known; means for safeguarding conventional equipment against these effects have already been developed. The major new hazard with laser equipment is the lasing output.

The damaging effects of CW laser radiation appear to be thermal in origin. For a ring laser gyro the area most sensitive to damage by such radiation is the eye. The region of the eye affected by the lasing depends on the wavelength of the radiation. The 0.633μ (or 1.15 μ) radiation from an He/Ne laser which passes through the pupil is focussed on and absorbed by the retina. As the incident energy increases in value, the reaction will proceed from a simple reddening to blistering, ulceration, charring, and finally disruption of the retina. Burns to the fovea, which makes up an area of the retina only about 1 mm in diameter, can result in serious impairment of vision. Burns in the remainder of the retina may not have as serious an effect, because the peripheral retina is mainly concerned with peripheral vision.

The main ring laser gyro output is not normally available for visual observation when the combining optics prism and photodiodes are in place. Even if it were, the output power is normally an order of magnitude or more less than the 1-millivolt value generally considered to be definitely dangerous to the eye. Any other ring laser gyro output (for example from a high reflectivity mirror or Brewster angle window) would be another order of magnitude smaller. In any case, however, exposure of the eye to any ring laser gyro output should be avoided, since the eye is a central nervous system organ, and, as such, cannot repair damage done to it.

From an analysis of the above hazard , information available from the literature (Ref 6-9), and safety requirem nts for electronic systems, the following safety recommendations are ma .e. Human factors aspects and safety in equipment operation are included as will be noted in the presentation. The recommendations are classified according to those which apply to the ring laser gyro sensor, the electronics, and the laboratory, maintenance facility or field location where the system is employed.

a. Ring Laser Gyro Sensor

1. The design and construction of the ring laser gyro should insure that all external parts, surfaces, and shields are at ground potential at all times.

2. If the ring laser gyro output beam is exposed, personnel should avoid looking into or along the axis of the beam, with or without protective eyewear. Personnel should also avoid looking at specular reflections of the beam.

3. The ring laser gyro sensor should be sealed to exclude dust and moisture from the optical elements.

4. An over-temperature sensor device should be employed to inhibit operation of the ring laser gyro when over-temperature conditions occur.

5. A plate should be attached to the instrument which provides the following information in a clearly visible location:

   a. Maximum ring laser gyro output power
   b. Operating wavelength

6. Personnel should become familiar with first aid techniques, particularly with artificial respiration techniques and the handling of electrical shock victims.

7. A ring laser gyro with an exposed output beam should be fixed in place so that inadvertent beam movement cannot occur if contact is made with the laser.

8. Standard operating procedures should be developed for each specific ring laser gyro operation and approved by the safety organization. Every step in the operating sequence should be documented in a checklist format and checked off in the proper sequence when operation is initiated.

9. Goggles or visors should be used when working with the ring laser gyro with its output beam exposed. Devices used for eye protection should be narrowband and centered at the ring laser gyro operating wavelength. Peripheral vision should not be impaired.

10. The ring laser gyro sensor should be surrounded with a shield to protect personnel against possible implosion. In most cases a thermal enclosure or magnetic shield already required will also serve this purpose.

11. Regular opthalmological examinations should be conducted for personnel working on ring laser gyros with exposed output beams.

12. The ring laser gyro system should be designed to withstand all environmental extremes anticipated (temperature, pressure, shock, vibration, etc.)

b. Ring Laser Gyro Electronics

1. The ring laser gyro electronics should be designed in modular form, with easy access to each module.

2. Test points should be provided for rapid malfunction isolation.

3. All high voltage terminals should be marked and shielded.

4. Voltage and current test points and adjustments should be located on a central, easily accessible, board.

5. Fast discharge should be provided for high-voltage circuits.

6. All modules with high voltages should be plainly marked.

7. Plug-in component boards should be used whenever possible.

8. Unless otherwise specified, meters should have provision for overload bypass or alternate protection to eliminate high voltage potential or current at the terminals in the event of meter failure.

9. All control shafts and bushings thereof should be grounded wherever practicable, or, alternatively, the control knobs or levers should be insulated from these shafts to prevent electrical shock or burns.

10. Overload protection for ring laser gyro electronics should be provided by fuses, circuit breakers, or other protective devices.

11. All electrical components used should comply with the appropriate military specifications.

12. Routing of wires and location of components should not impose undue mechanical strain on termination points.

13. All electrical connectors should be coded, keyed, or otherwise designed to avoid mechanical mismatching.

14. Connectors should have moisture and corrosion protection.

15. Contact of dissimilar metals should be avoided unless suitable corrosion protection is provided.

16. Critical circuits should be isolated where necessary to prevent degradation by signals from adjacent circuits which would result in an undesirable event.

17. Power and signal leads should not be routed through adjacent pins of connectors.

18. Sufficient working space should be allowed for engaging and disengaging connectors.

19. The ring laser gyro system electronics should be designed for the most severe environment the system will encounter.

20. Fuses should be designed so that they can be replaced without special tools. They should be located conveniently.

21. Terminals should be protected from shorting by foreign objects.

22. Switches and controls should be designed to prevent accidental activation.

23. Ground connection to shields and to other mechanical parts, except the chassis or frame, should not be made to complete electrical circuits because of possible inter-circuit interference. The path to ground from the equipment should:

    a. Be continuous and permanent.
    b. Have ample capacity to conduct safely any current imposed upon it.
    c. Have impedance sufficiently low to limit the potential above ground and to facilitate operation of the over-current devices in the circuit.
    d. Have sufficient mechanical strength to minimize the possibility of ground disconnection.

24. Ground connection to the chassis or frame should be mechanically secured by soldering to a spotwelded terminal on the ground wire and then securing the terminal by a screw, nut, and lockwasher.

25. Switchable protection should be provided to prevent contact with any moving mechanical parts when the equipment is operating.

26. Sharp projections on doors and similar parts should be avoided.

27. Doors or hinged covers should be rounded at the corners and provided with stops to hold them open.

c. Laboratory, Maintenance Facility, and Field Environment

1. Areas where ring laser gyros are used should be restricted areas.

2. The entrances to ring laser gyro use areas should be posted with warning signs.

3. When possible, a high general illumination should be maintained in ring laser gyro areas to keep the eye pupil diameter as small as possible.

4. Walls, ceilings, and interior window and door surfaces should be coated with non-reflecting material when practicable.

5. All areas should be adequately ventilated to prevent accumulation of oxides of nitrogen, ozone, hydrogen, or other toxic or flammable gases which may result from high voltage or chemical sources.

6. Components, parts, supplies, tools, and other equipment not in use during the setup or operation of ring laser gyros should be properly stored, leaving the area in an orderly condition.

7. In field use a decal or some other sort of marking should be utilized to warn personnel of the presence of the ring laser gyro. There should also be some means, such as an indicator light, to notify personnel when the ring laser gyro is on.

Although almost all the general and most of the specific system safety recommendations for a ring laser gyro system can be made at this time, several will escape notice until some Safety Testing is performed. At that time these will be identified, and also those design features employed to meet previously defined safety recommendations will be determined to be adequate or not. If complete safety testing is not economically feasible, partial design verification of safety characteristics would be demonstrated by laboratory test of a mockup or simulation approved by the procuring activity. Safety tests would be performed on critical components to determine the degree of hazard or the safety margin in the design. As an example, the high voltage circuitry needed for discharging the ring laser gyro must be checked to see that sufficient insulation is used, so that there is a negligible chance of breakdown or arcing occurring in normal system operation.

REFERENCES

1. W. R. Bennett, Appl. Opt. Supple, Opt. Masers 1962, p 24.

2. A. F. Wells, Structural Inorganic Chemistry, Oxford University Press, London 1962, 3rd ed.

3. J. E. Taylor, "Reliability Physics of Gaseous Optical Masers Using Noble Gas Active Media," Quantum Phys Lab Rpt. General Dynamics, Rochester, N.Y. (1965).

4. J. V. Martinez; "Influence of Plasma-Tube - Surface Interaction on he-ne Laser Lifetime" J. Appl. Phys. 37, 4477, Nov 1966.

5. L. F. Ehrke and C. M. Slack, J. Appl Phys. 11, 129, 1940.

6. Introduction to System Safety Engineering, Wiley, New York, 1971.

7. Air Force Manual 161-8, 1 April 1969.

8. System Safety Design Considerations for Air Force Laser Systems, Lt. Col. E. L. Thrush, June 1970.

9. MICOM Regulation Number 385-7, Safety Engineering Standard, Lasers, Lasers Supporting Equipment, and Facilities, 1 August 1967.

UNCLASSIFIED

Security Classification

DOCUMENT CONTROL DATA - R & D

(Security classification of title, body of abstract and indexing annotation must be entered when the overall report is classified)

1. ORIGINATING ACTIVITY *(Corporate author)*

Autonetics Division of Rockwell International Corporation
Anaheim, California

2a. REPORT SECURITY CLASSIFICATION

Unclassified

2b. GROUP

3. REPORT TITLE

RF Cleaning – Ring Laser Gyro

4. DESCRIPTIVE NOTES *(Type of report and inclusive dates)*

Final Report, 17 April 1972 through 28 February 1973

5. AUTHOR(S) *(First name, middle initial, last name)*

Gary D. Babcock, Fredrick Vescial

6. REPORT DATE	7a. TOTAL NO. OF PAGES	7b. NO. OF REFS
June 1973	85	9

8a. CONTRACT OR GRANT NO.	9a. ORIGINATOR'S REPORT NUMBER(S)
F53615-72-C-1741	C73-600/201
b. PROJECT NO.	
c.	9b. OTHER REPORT NO(S) *(Any other numbers that may be assigned this report)*
d.	

10. DISTRIBUTION STATEMENT

Distribution limited to U. S. Government agencies only; report covers test and evaluation of military hardware; June 1973, other requests for this document must be referred to AFAL/NVN, Wright-Patterson AFB, Ohio 45433.

11. SUPPLEMENTARY NOTES	12. SPONSORING MILITARY ACTIVITY
	United States Air Force Air Force Systems Command Hq 4950th Test Wing 4950/PMEB Wright-Patterson AFB, Ohio 45433

13. ABSTRACT

This document presents the results of RF Cleaning - Ring Laser Gyro program performed by the Autonetics Division of Rockwell International Corporation. One of the most significant problems confronting ring laser development is short life. The key to long ring laser life is a clean cavity (free of contaminants). The objectives of the contract were to test the RF cleaning concept and to build deliverable RLG hardware including both sensors and electronics.

The RF cleaning study was performed to determine the feasibility of using RF energy to clean ring laser gyro cavities. A "dual discharge" approach was selected as the most suitable RF coupling technique for cavity cleaning. Experimental studies were conducted to select and optimize cleaning parameters and procedures. Comparative effectiveness of cleaning techniques was measured by optical spectroscopy and by life test of operational ring laser instruments.

Data are presented which indicate that oxygen is the most efficient cleaning gas and that RF cleaning used in conjunction with normal thermal degassing processes can provide for improved laser gyro cleanliness. Conclusions and recommendations for future studies are also presented.

Instrument and electronic design of the deliverable hardware are described. Autonetics state-of-the-art design and processing techniques are incorporated in the sensor design. Operating procedures and test results obtained with the equipment at Autonetics are given. A summary is presented of brief studies conducted on RLG reliability, maintainability, and system safety.

DD FORM 1 NOV 68 1473

UNCLASSIFIED

Security Classification

14. KEY WORDS	LINK A		LINK B		LINK C	
	ROLE	WT	ROLE	WT	ROLE	WT
Laser Gyro						
Ring Laser Gyro						
RF Discharge Cleaning						